TÉCNICO LISBOA

Optimization of chemical vapor deposited (CVD) graphene transfer for nanopore devices

Telma Daniela Azevedo da Silva Oliveira

Thesis to obtain the Master of Science Degree in

Bioengineering and Nanosystems

Supervisor(s): Stephanie Heerema
Prof. Luis Joaquim Pina da Fonseca

Examination Committee

Chairperson: Prof. Raúl Daniel Lavado Carneiro Martins
Supervisor: Prof. Luis Joaquim Pina da Fonseca
Member of the Committee: Prof. Susana Isabel Pinheiro Cardoso de Freitas

December 2015

Acknowledgments

Firstly, I would like to express my gratitude to Prof. Dr. Cees Dekker for giving me the opportunity to join the Graphene Nanopores group and work on such amazing facilities, with great people. I would also like to thank my supervisor Stephanie Heerema for the training I received, for the help and advices that she gave me throughout the months I spent in the BN department. My sincere thanks goes also to the Kavli Nanolab Staff for their kindness and availability in the clean room.

Besides the scientific knowledge that I acquired, what I value the most about my college experience was the people I got to know and all the moments we shared together. I would like to thank all the friends I made throughout the years for their guidance, companionship and for the great times we had together. These are memories that I shall hold dearly.

This last acknowledgment is for my parents, sister and aunt, for making all my accomplishments possible. Therefore, I would like to express my profound gratitude for their unconditional love, encouragement and patience.

Resumo

Nanoporos são orifícios nanométricos numa membrana impermeável utilizados como uma ferramenta de sequenciação de ADN. A entrada e saída de ADN do poro causa picos na corrente iónica, produzindo um sinal a partir do qual a sequência de ADN poderá potencialmente ser determinada. A utilização de uma membrana de grafeno possibilita a detecção de um nucleótido de cada vez, por possuir espessura atómica. Grafeno obtido por deposição química de vapor apresenta a vantagem de produzir uma monocamada contínua. Para ser utilizado em membranas de nanoporos, o grafeno obtido por deposição química de vapor tem de ser transferido do substrato de metal em que foi depositado para o substrato pretendido. A transferência é usualmente realizada utilizando um suporte polimérico. No entanto, este método frequentemente produz quebras e acumulação de resíduos poliméricos no grafeno. A influência dos parâmetros da transferência na morfologia e estrutura do grafeno foi estudada. Imagens obtidas com o microscópio óptico e microscopia de força atómica mostraram que a adição de um passo de cozimento após o revestimento com PMMA, conduziu a melhorias na densidade de partículas e dos parâmetros de rugosidade. Resultados semelhantes foram obtidos adicionando uma etapa de cozimento após o filme de grafeno/PMMA ser transferido para o substrato final. Um aumento do tempo de permanência dos filmes em água durante o passo de limpeza em ácido hidroclorídrico levou uma dimuição de resíduos de PMMA e melhorias na rugosidade. Exposição das amostras a temperaturas elevadas reduz significativamente a densidade de resíduos de PMMA.

Palavras-chave: nanoporos, grafeno, deposição química de vapor, transferência com suporte de PMMA, microscopia de força atómica

Abstract

Nanopores are nanometer scaled holes in an impermeable membrane and have been studied with the purpose of sequencing DNA. DNA entering and exiting the pore causes dips in the ionic current, providing a signal from which the DNA sequence could potentially be obtained. A graphene membrane opens up the possibility of single nucleotide detection, due to its single-atom thickness. CVD graphene has been studied as an alternative to exfoliated graphene because of its large carbon monolayer which has many advantages to the small graphene flakes obtained by exfoliation, which are difficult to produce. To be used in nanopore membranes, CVD graphene has to be transferred from the metal substrate in which it was grown to the desired substrate. This is frequently accomplished using a polymer support to transfer the graphene to the measuring device. However, breaks and polymer residues are frequently found in the membrane. The impact of transfer parameters on graphene morphology and structure was studied. Optical microscopy and atomic force microscopy showed that addition of a baking step after PMMA spin coating lead to improvements in particle density and roughness parameters. Similar results were obtained by addition of a baking step after graphene/PMMA films transfer to the final substrate. Longer deionized water steps during hydrochloric acid cleaning also reduced particle density and roughness was improved. Also, annealing the samples at high temperatures highly reduced PMMA residue density.

Keywords: nanopores, graphene, chemical vapor deposition, PMMA transfer method, atomic force microscopy

Contents

List of Tables

List of Figures

List of Acronyms

AFM - **A**tomic **F**orce **M**icroscope

APCVD - **A**tmospheric **P**ressure **C**hemical **V**apour **D**eposition

CNT - **C**arbo**n**ano**t**ubes

CVD - **C**hemical **V**apour **D**eposition

DI - **D**e**i**onized

DNA - **D**eoxyribo**n**ucleic **A**cid

HCl - **H**ydrogen **C**hloride

HOPC - **H**ighly **o**rdered **p**yrolytic **g**raphite

LPCVD - **L**ow **P**ressure **C**hemical **V**apour **D**eposition

PDMS - **P**olyd**i**methyl**s**iloxane

PMMA - **P**oly**m**ethyl **m**eth**a**crylate

UHV - **U**ltra **H**igh **V**accum

Chapter 1

Introduction

1.1 Nanopore devices for DNA sequencing

Knowledge of DNA sequences of different organisms contributed to significant advances in biological research, leading to major breakthroughs in the fields of medicine and biotechnology [1]. The first methods for DNA sequencing emerged in the early 70s, with Sanger sequencing [2]. Since then, several techniques have been developed, that require extensive amplification and labeling steps, such as microarrays [3, 4], in which the complementary of the DNA strand to be sequenced is immobilized on a solid substrate, and the sequence is determined by nucleotide addition. In the last decade, nanopore based devices have been subject of substantial research for the purpose of sequencing DNA, since they do not require amplification or labeling [5, 6].

As presented in figure 1.1, the principle behind nanopores is that a nanoscale hole is made in an impermeable membrane [7]. Voltage application across the pore causes ion migration, leading to electric current that will be measured. Transient changes in the ionic current can be associated with pore occupation by a macromolecule, therefore, the translocation of a molecule through a pore can be sensed by these changes [8, 9, 10].

In the last decade, considerable nanopore research has been pursued on different types of nanopores. Biological nanopores are composed by a pore-forming protein in a membrane such as a lipid bilayer [11, 12]. Subsequently, solid-state nanopores emerged as an alternative to biological nanopores, since they possess features such as mechanical robustness, well-defined and tunable geometry and compatibility with measuring devices [13].

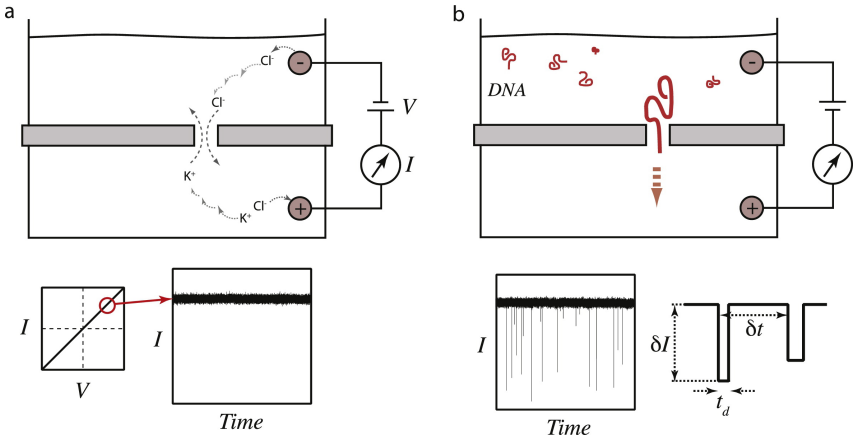

Figure 1.1: Fundamentals of nanopore measurements. (a) Voltage application across a nanopore causes ionic current. The current is proportional to the voltage. (b) Obstruction of the pore, in translocation events, results in pulses. Adapted from [8].

Silicon-based membranes have been studied as substrates due to their high chemical stability and low mechanical stress[14]. However their use for DNA sequencing is not straight forward, since they are relatively thick, typically around 30nm, which corresponds to 60 bases along a single stranded DNA molecule [15]. This limitation can be surpassed with graphene nanopores. Graphene is a single atomic layer of carbon atoms, arranged in a honeycomb-shaped lattice. Due to its notable electrical [16], chemical [17, 18] and mechanical [19, 20] properties such as high Young's modulus, large specific surface area and high electrical and thermal conductivity, graphene applications have been deeply studied [21, 22]. Being about 0,3 nm thick, it discloses the possibility of single base detection of DNA, as represented in figure 1.2 [15].

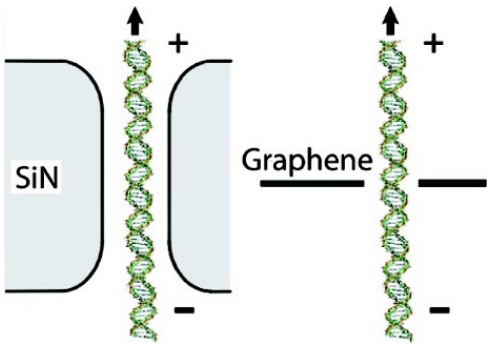

Figure 1.2: DNA translocation in a silicon nitride nanopore and in a graphene nanopore. Adapted from [15].

Initially, graphene sheets were obtained by graphite exfoliation, either by rubbing small graphite crystals against each other or simply using tape [23, 24, 25]. Despite the simplicity of the process, the main issue with it was the difficulty in identifying suitable graphene sheets. Monolayer graphene flakes are quite rare and small. Most of the of the formed flakes possess several layers of carbon [16]. A possible solution for this obstacle is the production of CVD (chemical vapor deposited) graphene, by decomposing carbon compounds in a metal surface. With CVD it is possible to produce large areas of monolayer graphene.

However, CVD graphene requires the removal of the metal and a transfer process, which may cause the graphene to deteriorate [26].

1.2 Master project outline

The experimental part of this project was carried out in the Kavli Nanolab Delft facilities, under the supervision of MSc. Stephanie Heerema and Prof. Dr. Cees Dekker from the Bionanoscience Department of TU Delft.

In this project the transfer of CVD graphene by the PMMA method was studied. Various irregularities such as wrinkles, breaks and polymer residues occur in this type of transfer, deteriorating graphene quality. Various modification on the process were proposed in order to improve the quality of the transfer. Thus, it was carried a transfer with a polymer-free method.

In the first chapter, the synthesis and transfer of graphene produced by CVD will be discussed. To comprehend the influence of CVD synthesis on graphene quality, the kinetics of graphene growth and other parameters will be empathized. Thus, the transfer is process greatly influences CVD graphene quality, therefore different approaches to the transfer process are mentioned.

In the second chapter is presented a description of the materials, methods and equipments used during this project. Also, the standard PMMA method transfer is fully described.

In the third chapter, an analysis is carried out on the resulting AFM images, obtained from CVD graphene transfered with the standard PMMA methods and the modifications. Particle and roughness analysis were performed on each image, and the obtained parameters will be discussed.

Chapter 2

Theory

2.1 Graphene synthesis by chemical vapor deposition

The principle behind chemical vapor deposition is that the substrate is exposed to gaseous precursors, which when in contact with the substrate at high temperatures, will deposit on its surface, creating a thin film [27]. The quality of the materials obtained by CVD is strongly dependent on the process parameters such as gas temperature, pressure, and time duration. To achieve single layer graphene by CVD, with quality similar to exfoliated graphene, these parameters have to be adjusted to the deposition process. Also, the metal used as substrate will influence the global process. Transition metals such as copper, nickel, platinum, ruthenium and iridium have been used to grow CVD graphene, however copper is more commonly used for this specific purpose [28, 29, 30, 31].

2.1.1 Kinetics of graphene growth

The process of the CVD graphene film formation consists of four major steps: heating, annealing, growth and cooling, as it is shown in figure 2.1. The process occurs inside a CVD chamber, and starts with substrate heating to 1000 ^{o}C to boost the pyrolysis (thermochemical decomposition of an organic material at elevated temperatures [32]) of the precursor hydrocarbons gas, usually methane or propane. Afterwards, the elevated temperature promotes the formation of larger grain sizes and smoother surfaces. The third step consists of the pyrolysis of the precursor gas that is added into the chamber. Finally, the gas supply is closed and the chamber is cooled down to room temperature [28].

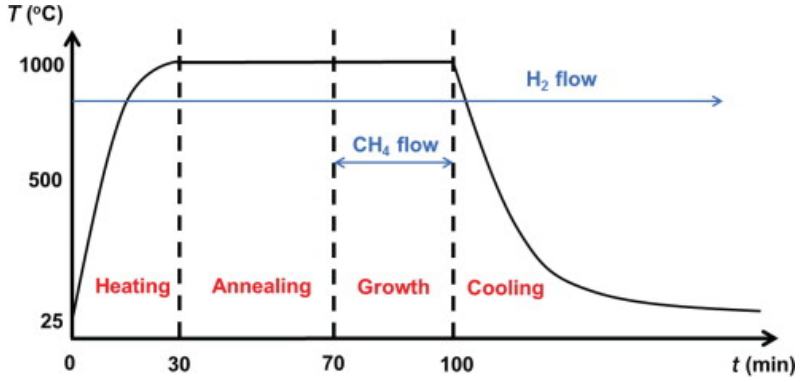

Figure 2.1: Flow of graphene growth by CVD. The process consists of heating, annealing growth and cooling. Hydrogen flows throughout the entire process. In the growth phase hydrocarbon gas is supplied. Adapted from [28].

The growth kinetics of graphene on a metal is determined, not only by chamber temperature and pressure, but also by metal's properties such as crystalline structure and carbon solubility on the metal. The latter has a significant influence on the process, since, if the carbon has low solubility on the metal, graphene formation will be limited to the metal surface. On the other hand, if carbon solubility in the metal is high, two processes will occur simultaneously: diffusion of carbon into the metal film during growth, and carbon precipitation upon cooling after synthesis. [33, 34].

As seen in figure 2.2, graphene growth on metal comprises 6 steps: (1) diffusion of the hydrocarbon gas from the bulk layer to the surface; (2) adsorption of the molecules on the surface; (3) decomposition of the molecules to form active carbon and hydrogen species; (4) formation of graphene lattice by surface diffusion of the active species; (5) desorption of inactive hydrogen species and formation of hydrogen gas; (6) diffusion of hydrogen gas from the surface to the bulk region [34].

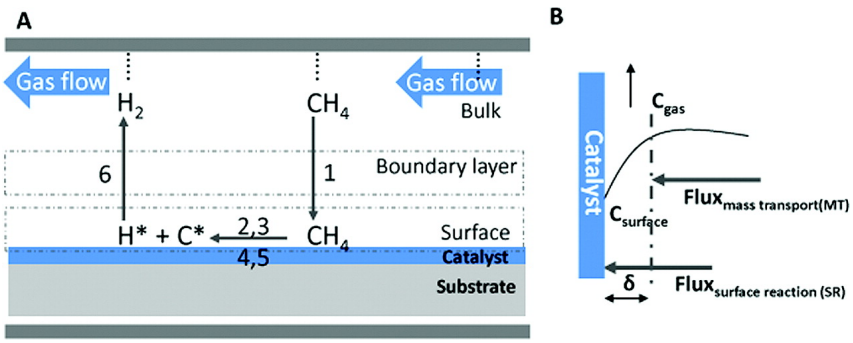

Figure 2.2: (a) Graphene growth mechanism by CVD; (b) Mass transport and surface reaction fluxes in steady-state. The boundary layer thickness is represented by δ. Adapted from [34].

The process of graphene growth can be categorized in two different regimes: a mass transport regime where the species diffuse through the boundary layer (1,6); and the surface reaction regime that comprises the reactions occurring in the surface region (2-5). Thus, two different regimes translate into two

different fluxes. Equations 2.1 and 2.2 define each of both fluxes involved in this process:

$$F_{mass\ transport} = h_g(C_g - C_S) \tag{2.1}$$

$$F_{surface\ reaction} = K_S\ C_S \tag{2.2}$$

where $F_{mass\ transport}$ and $F_{surface\ reaction}$ are the mass transport and the surface reaction fluxes (respectively), h_g is the mass transport coefficient, C_g corresponds to the concentration of hydrocarbon gas in the bulk region, C_S is the concentration of the active species in the surface region and K_S is the surface reaction constant [34]. For steady-state conditions, the fluxes can be written in equation 2.3.

$$F_{total} = F_{mass\ transport} = F_{surface\ reaction} = C_S\ \frac{K_S\ h_g}{K_S\ +\ h_g} \tag{2.3}$$

Both fluxes occur simultaneously and the rate-limiting step of the process determines the speed of the process [35]. Thus, the graphene growth process can occur in 3 different regimes:

- reaction is limited by mass transport if $K_S \gg h_g$;
- reaction is limited by surface reaction if $K_S \ll h_g$;
- mixed reaction if $K_S \sim h_g$.

Graphene synthesis by CVD has been performed in atmospheric conditions (APCVD) and also in low pressure (LPCVD) or high vacuum conditions (UHV) [36, 37]. From Fick's Law of diffusion, h_g can be expressed as a function of the diffusion coefficient, D_g, and the boundary layer thickness, δ, as described in equation 2.4.

$$h_g\ =\ \frac{D_g}{\delta} \tag{2.4}$$

To obtain high quality CVD graphene it is necessary that graphene growth is self-limiting, and also that it is grown in the surface reaction regime, to avoid the boundary layer effects. In this regime, the surface reaction constant (K_s) is negligible if compared with mass transport coefficient (h_g). From equation 2.4, an higher h_g translates into an higher diffusivity. Since at lower pressures the diffusivity coefficient is higher, lower pressure conditions (LPCVD or UHV) favor the growth of uniform and defect free single layer graphene. On the other hand, if graphene is grown under atmospheric conditions, graphene growth is not self-limiting. The boundary layer thickness and the amount of active species diffusing from the bulk region to the surface will variate, resulting in an non-uniform graphene growth [34].

2.1.2 Graphene nucleation

In section 2.1.1 are reported the effects of process parameters in kinetics of graphene growth. It is in the first stages of growth that these parameters have a fundamental role on graphene structure. After pyrolysis of the precursor gas, usually methane, carbon species aggregate in the metal surface forming several carbon nuclei, that will grow with time, and eventually meet, forming boundaries. These boundaries are associated with structural defects, degrading significantly graphene quality. Defect density decrease is obtained by producing graphene with bigger domains and less nuclei [38].

The effect of temperature (T), methane flow rate (J_{Me})and methane partial pressure (P_{Me}) on nucleation density and domain size of CVD-graphene grown on copper is described in figure 2.3.

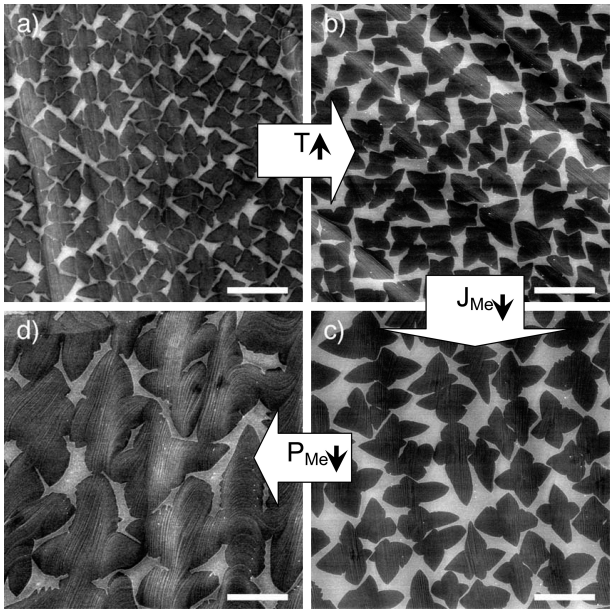

Figure 2.3: SEM images of partially grown graphene flakes and process parameter effects on nucleation and growth. From (a) to (b), the temperature was increased; from (b) to (c) the methane flow rate was increased; from (c) to (d) methane pressure was decreased. Adapted from [39].

As described in reference [39], graphene growth on copper follows 5 sequential steps: (1) copper exposure to hydrogen and methane, (2) decomposition of methane on copper surface by catalysis, (3) copper surface is either undersaturated, saturated or supersaturated with hydrocarbon species, depending on process parameters, (4) Formation of graphene nuclei and growth of graphene domains, (5) full copper coverage. When copper surface is undersaturated, there are not enough hydrocarbon species for the carbon to nucleate on copper surface, therefore graphene formation does not occur. If copper surface is saturated, carbon nuclei are formed, but the amount of hydrocarbon species is not enough for the graphene domains to grow and form boundaries. If copper surface is supersaturated, graphene islands grow until they reach another island, due to methane availability.

To grow continuous graphene with larger domain size a two-step methodology has been pursued. First,

nuclei are formed in high temperatures at low methane flow rate and low methane parcial pressure. Subsequently, methane flow rate and pressure is increased to obtain full coverage [39].

Temperature and copper surface morphology also have considerable influence on graphene nucleation and growth. In a smooth surface, two different regimes of graphene growth have been reported. Below 870^o C, nucleation rate is limited by capture of carbon adatoms (atoms that lie on a crystal surface) by a nucleus. Above 870^{o}C, nucleation is controlled by desorption. In both conditions, increasing temperature leads to decreasing nucleation density. It has been observed that the nucleation density can be higher in a uniform substrate than in the flat area of an substrate with both flat and rough regions [40].

2.1.3 Influence of metal substrate on graphene growth

To grow single layer graphene the most commonly used substrate is copper, due to its negligible carbon solubility at growth temperature [41]. For this purpose, graphene is usually grown on a 25 μm thick polycrystalline copper foil with at least 99,8% purity [42]. Copper crystalline structure affects the mechanism of graphene growth, and its morphology. It has been observed that, copper grain boundary is not usually a favored site for graphene nucleation, and that carbon atoms cross nuclei boundary lines [43]. Furthermore, copper impurities and defects are more favorable sites for nucleation. In order to improve graphene quality by lowering graphene nucleation density, the frequency of these sites has to be diminished. To achieve high quality graphene, copper with higher purity (99,9995%) has been used, however the cost of this material is high [44]. Another option is to perform pre-treatment on copper substrates. Annealing copper substrate before deposition as shown to increase copper grain size and to decrease defects, due to rearrangement of atoms on the surface [45]. Copper substrate is covered by oxides that reduce its catalytic activity. To remove them, the copper surface has been annealed and also chemical treatments with acetic acid have proved to be effective [46].

2.2 Graphene Transfer methods

To be used in electronics devices, graphene deposited in a metal substrate has to be transfered to the desired substrate. Not only the growth process influences graphene quality, but also the transfer methods, since graphene quality can deteriorate during the transfer. This process involves the use of a support layer, such as PMMA or PDMS, leading to residue accumulation on the graphene layer. Also, wet etchants, such as ferric chloride ($FeCl_3$), ferric nitrate ($Fe(NO_3)_3$) and ammonium persulfate ($(NH_4S_2O_8)$), are used to remove the metal substrate such as nickel or copper, however besides leaving

residues on the graphene it can also break and ripple this layer [47].

2.2.1 Polymer supported transfer

A possible approach to graphene transfer requires the use of a supporting layer. Since graphene is a single atomic layer of carbon atoms, a support would protect and strengthen it. A successful transfer requires the use of a support layer that does not damage the graphene and that is resistant to the wet etchant [47].

PDMS (polydimethylsiloxane)

PDMS is a polymer material widely used, not only in soft lithography, but also for graphene transfers. This polymer is robust, moldable and resistant to a variety of etchants. It has a low surface adhesion force, facilitating the PDMS detachment from graphene transfered to the desired substrate [48]. Since PDMS is weakly bounded to the target substrate, but adheres strongly to graphene, it is suitable for the transfer process. The graphene transfer starts with application of the graphene/metal stack to a PDMS cast. This structure is then floated in a etchant bath, to selectively remove the metal. The PDMS acts as a metal support to the graphene during the etching. After the metal is etched, the PDMS/graphene structure is pulled out of the bath, rinsed and dried. Subsequently, the PDMS/graphene stack is brought into contact with the substrate, and since PDMS-graphene bounds are weaker than those made with the target substrate, the graphene is transferred and the PDMS is released. [33]. This PDMS transfer process is described in figure 2.4.

Another technique performed to obtain patterned graphene for device making, requires the use of a pre-patterned graphene PDMS mould. With this stamping method the risk of rupture is decreased, if compared the pre-patterned metal technique. Thus, instead of growing graphene in a patterned metal, PDMS was molded with the desired pattern in one of its surfaces. After metal etching, the remaining graphene on PDMS graphene was stamped on the target substrate. In figure 2.5 is shown the schematics of micro-patterning using PDMS mould [49]. Since PDMS stamping using monolayer graphene grown in a copper substrate has been challenging, due to breaking and rupturing of the membrane, it has been suggested that this technique may be more suitable for multilayer graphene. PDMS transfer is not as widely used as PMMA transfer, nevertheless it is an frequent alternative for applications requiring patterning for soft-lithography [28].

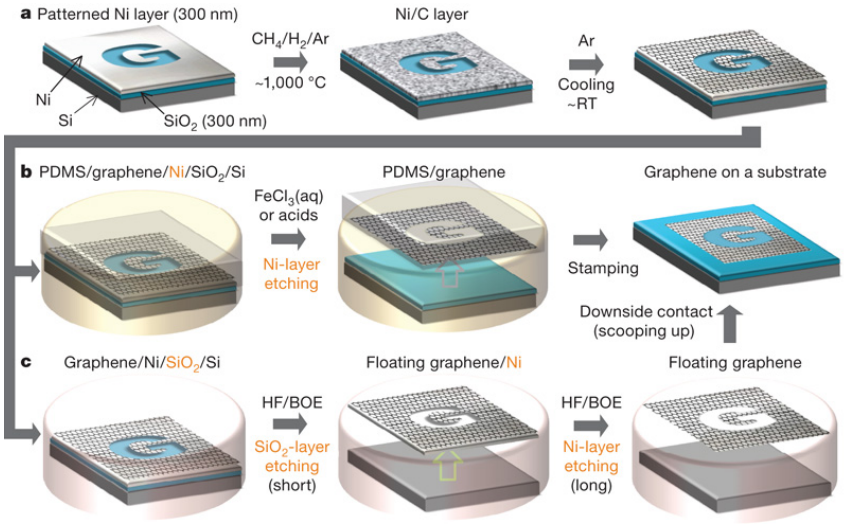

Figure 2.4: Transfer of CVD graphene grown in a metal substrate using PDMS. (a) Synthesis of graphene on a metal substrate; (b) Metal etching using ferric cholrid or acids and graphene transfer to substrate; (c) Etching using buffered oxid etchant (BOE) or hydrogen fluoride (HF) solution and graphene transfer. Adapted from [33].

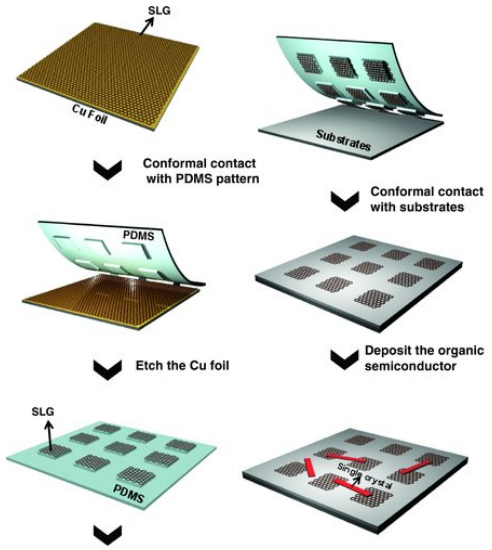

Figure 2.5: Transfer of CVD graphene grown films in a metal substrate using a PDMS stamp. Adapted from [49].

PMMA (poly(methyl methacrylate))

PMMA is the most widely used polymer for CVD graphene transfer [29]. This polymer had already been used in CNT's transfer process [50]. PMMA covalently bounds to graphene, providing a better support for the carbon layer, leading to less cracking and rippling than PDMS. However, since the bounds between PMMA and graphene are stronger, it is more difficult to remove the polymer layer [30]. In figure 2.6 is described the classic PMMA transfer process. First, PMMA is spin coated on to graphene grown in a metal (or in $Si0_2$)[29]. Polymer thickness can be adjusted with the spinning rate and the PMMA concentration. A similar procedure as also been carried out in HOPG (highly ordered pyrolytic graphite) flakes

on $Si0_2$/Si [51]. A baking step can be introduced to evaporate the solvent on the PMMA/graphene/metal stack. If the graphene layer is grown by CVD, both sides of the copper foil will have graphene on it. Therefore, a plasma etching step is required to remove the carbon layer in one of the metal sides, or else graphene residues may deteorate the graphene. To remove the metal layer, the stack is placed on a metal etchant, and after the metal is fully etched, the PMMA/graphene is scooped out, placed on DI water and rinsed several times. Also, diluted hydrochloric acid (HCl) is often used to further remove metal etchant residues. After these cleaning steps, the PMMA/graphene stack is scooped out and transfered to the desired substrate (such as a SiO_2/Si wafer). The excess water may be removed with using a nitrogen gun. The stack may dry in air for a few hours, or it can be baked to evaporate the remaing water. To remove the remaining PMMA layer, the stack is placed in a acetone bath or it can be annealed in vacuum or in a N_2, Ar, H_2, or a combination of those atmosphere.

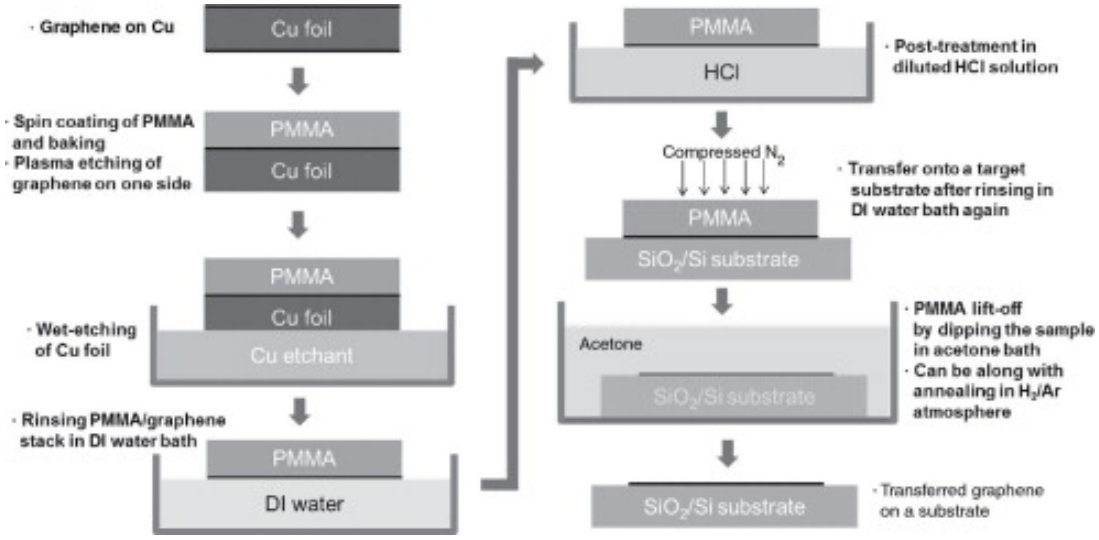

Figure 2.6: Transfer of CVD graphene grown films the classic PMMA supported transfer. Adapted from [49].

To improve the quality of the PMMA transfer and avoid degradation, various adjustments and optimization to the classic process have been carried. Although with PMMA is possible to obtain a graphene layer with improved continuity, if compared to PDMS, some breaks and wrinkles still occur, specially in monolayer graphene. It has been assumed that they are caused by wrinkles and other defects that appeared in copper during the CVD growth process [52]. A second PMMA layer approach has also been studied to reduce the breaking, rupturing and wrinkling of the graphene membrane. Improvements in transfer quality have been reported by adding an additional PMMA layer to dissolute the first one [53].

Thus, graphene quality is also deteorated by PMMA residues that remained attached to the graphene after the acetone bath. These residues are difficult to remove since PMMA covalently bonded to graphene. Combined with breaking and wrinkling, these residues remarkably deteriorate the electrical and physical properties of graphene, decreasing carrier mobility [54]. Graphene annealing has been used after the

acetone bath to address this issue. Improvements have been reported with graphene annealing performed in UHV (ultra high vacuum) conditions and in vacuum furnace at 200-500 ^{o}C [55, 56, 57, 58]. However, if carried at very high temperatures it lead to degradation of graphene's electrical properties [59].

2.2.2 Large-scale continuous tranfer

Thermal release tape has been used as an alternative to polymers in the transfer of graphene grown epitaxially on a silicon carbide (SiC) substrate. With a steel pressure plate, the tape is applied on graphene and, by the force of the adhesive, graphene is pulled out from the substrate. To obtain the graphene on the desired substrate, heat must applied to release the tape [60].

A promising application of thermal release tape is in the roll-to-roll transfer of CVD graphene to a flexible substrate. While polymer use is convenient in wafer scale transfers, with roll-to-roll approach is possible to transfer graphene with a 30 inch diagonal dimension. Because of its scalability, roll-to-roll transfer is suitable for industrial processes. This type of transfer usually starts with CVD graphene adhesion to the tape, followed by metal layer etching and finally, graphene is released and transfered to the desired substrate [61, 62, 63]. In figure 2.7 is shown the schematics of the process. After graphene is grown by CVD on a roll of copper foil inside a thermal reactor, the graphene film is attached to the thermal release tape. Copper is etched in a bath with metal specific etchant. Graphene on the tape is moved across the two rollers together with the desired substrate, and exposed to modest heating (around 120^{o}C). The heat removes the tape's adhesiveness and promotes substrate adhesion to graphene. With this technique is possible to transfer several layers of graphene, by repeating the process. [64].

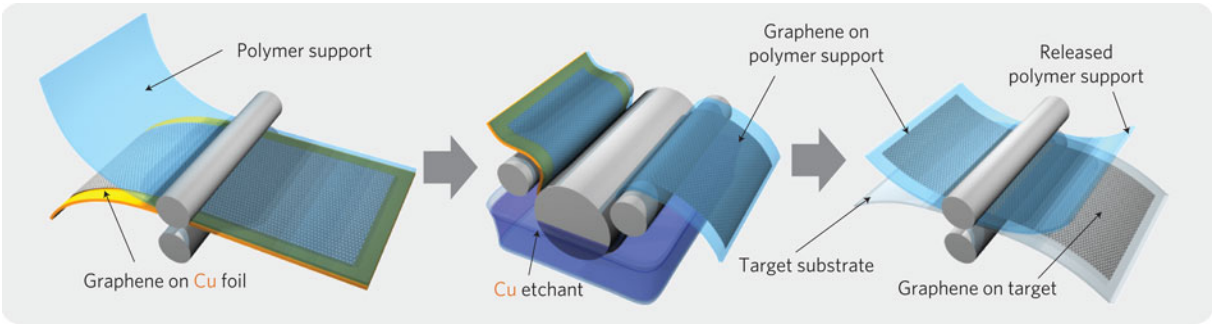

Figure 2.7: Roll-to-roll transfer of graphene grown by CVD. Adapted from [64].

Roll-to-roll transfer is used in the transfer of graphene to flexible substrates. To transfer CVD graphene to a rigid substrate, another method using also thermal release tape as been proposed: the hot pressing method. The process is similar to the roll-to-roll transfer, but a large hot plate is used instead of the heated rollers. With this transfer there is no risk of ripping the graphene by shear stress.

Thermal release tape is attached to the graphene film, followed by copper etchant bath. Finally, the tape/graphene/substrate is placed in the hot press, causing the tape to lose adhesion force, finalizing the transfer [65].

2.2.3 Transfer-free graphene growth & polymer-free transfer

CVD graphene transfer is usually carried out using the PMMA method. However, quality of the transfer may be deteriorated due PMMA residues accumulation and membrane rupturing. To surpass these issues, several approaches in which no polymer is used as a support for the transfer, have been proposed.

A possible approach is to grow graphene between a metal layer and the target substrate. During graphene growth, carbon atoms travel through copper grain boundaries, and graphene is synthesized underneath the metal layer. After graphene synthesis, the copper layer is removed with tape or using copper etchants [66]. Graphene has also been grown on a Si/SiO_2 substrate, by heating vinyl polymers under a metal substrate [67]. Both processes are described in figure 2.8.

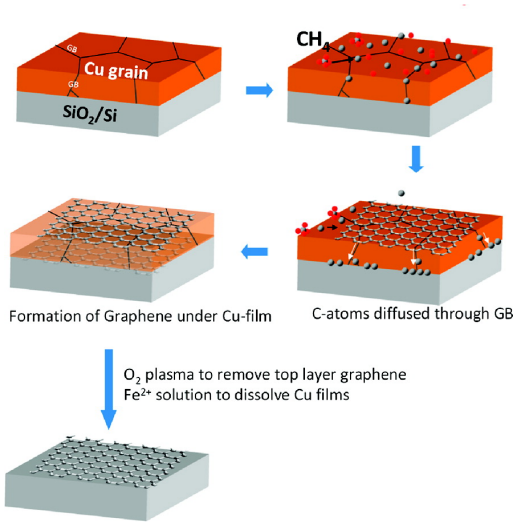

(a) CVD graphene synthesis by diffusion carbon atoms through copper boundary .

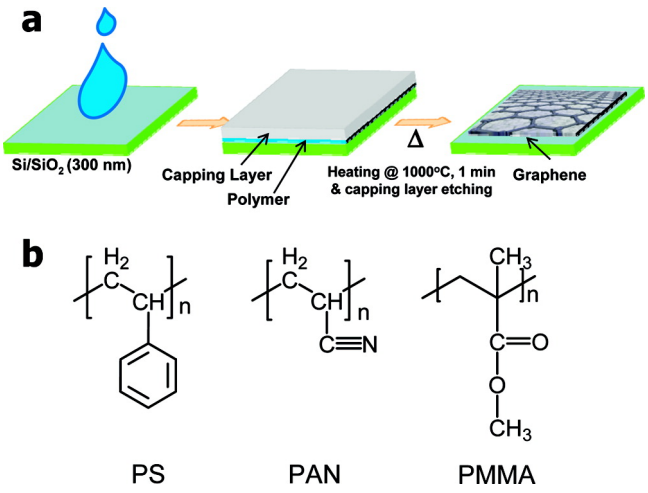

(b) CVD graphene synthesis by vinyl polymer pyrolysis and polymers used in the studies described in reference [67].

Figure 2.8: Graphene growth between a metal substrate and a Si/SiO_2 substrate. Adapted from [66, 67].

Graphene as also been grown in copper deposited on dielectric surfaces such as quartz. Instead of using the typical metal etchant bath, copper is removed by dewetting and evaporation of the copper layer. The graphene/copper/substrate was kept at high temperatures from 15 minutes to 7 hours. Despite the fact that it takes more than 6 hours to evaporate the copper, it has been shown that graphene quality starts deteorating after 2 hours [68].

In figure 2.9 is described a CVD graphene transfer without the use of any polymer as a support for the

graphene membrane. Graphene grown on copper is placed with a thin graphite holder in a metal etchant solution to remove the copper. The holder is used to prevent graphene from ripping apart due to surface tension. After the copper is completely etched, the graphene should be floating in the etchant solution. Using a pump system, the etchant is pumped out from the container while and IPA is pumped in. The desired substrate is placed on the bottom of the container and the IPA solution is pumped out, lowering the graphene to the substrate [69].

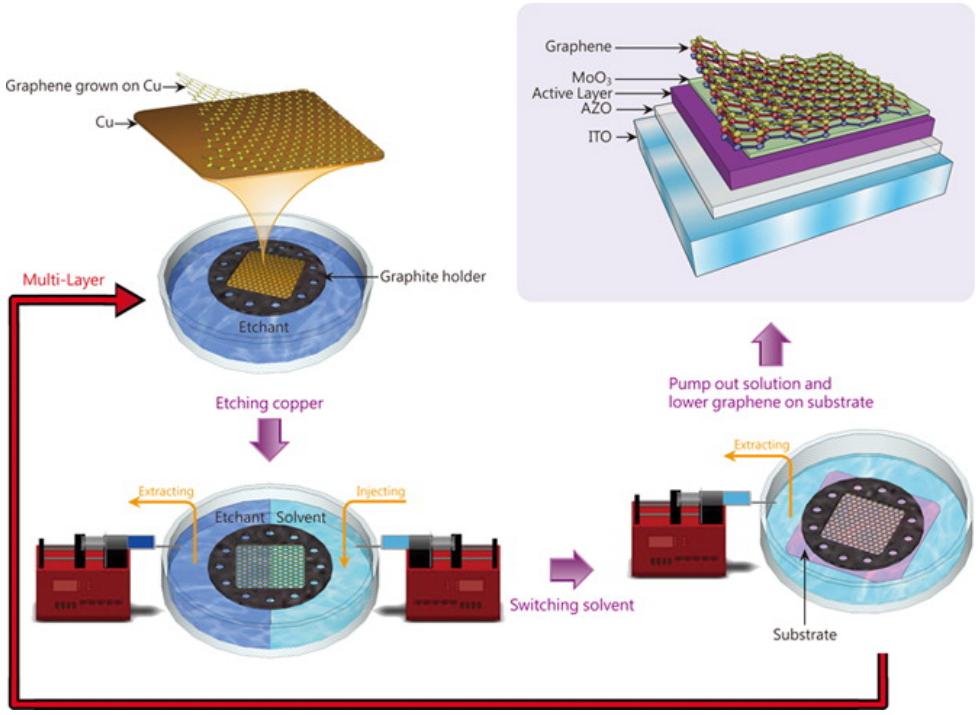

Figure 2.9: Polymer-free transfer of CVD graphene to a target substrate. Adapted from [69].

Chapter 3

Methods

3.1 Materials and equipments

3.1.1 Materials

The materials used to perform the transfers in this work were:

- CVD graphene

  Copper thickness: 36 μm;
- Si/Si0_2 wafers;
- PMMA A6 950K (6 % in anisole and molecular weight 950K);
- Ferric chloride based copper etchants:

  Copper etchant by Sigma Aldrich;

  PC copper etchant -100 by Transene;
- Hydrochloric acid by Sigma Aldrich ;
- FastScan-A Bruker AFM probe.

3.1.2 Equipments & Software

The equipments used in this work transfers were:

- Spin coater Suss Microtec Delta 8;

- Hot plate
- PVA TePla 300 Microwave Plasma System;
- Optical microscope Leica INM20;
- Bruker AFM (atomic force microscope);
  Nominal radius of the tip: 5 nm;
- NanoScope 1.5 analysis software.

3.2 CVD graphene transfer

3.2.1 Standard PMMA transfer

The standard PMMA transfer starts with spin coating of a A6 PMMA layer on a 5$\times$5 mm graphene/copper/ graphene piece (4000 rpm, 1 min, for a 500 μm thickness), followed by cleaning the backside of the copper foil with a small amount of acetone in a cotton wipe, to remove PMMA residues accumulated during spin coating. The PMMA cure was made at room temperature during 10 minutes. To remove the graphene from this of the copper foil, the stack is plasma etched for 10 seconds (oxygen flow: 200ml/min, power: 50W). In order to etch the copper foil, the PMMA/graphene/ copper/graphene films were immersed on Sigma Aldrich copper etchant for 5 hours or in Transcene CE-100 for 2 hours. After the copper is completely removed, the PMMA/graphene films are transfered to a 1:10 mixed solution of HCl during 20 minutes and then rinsed 3 times in DI (deionized) water, during 20 minutes each time. After HCl cleaning, the films are transfered to a Si/SiO_2 wafer and dried in air for 2 hours. Finally, to remove the PMMA, the PMMA/graphene/Si/SiO_2 stack is placed in a acetone bath for 10 minutes. The Si/SiO_2 wafers were previously plasma cleaned in the Tepla 300 under an oxygen flow of 200 ml/min, 500W for 1 minute. Schematics of the process is represented in the figure from image 3.1.

3.3 CVD graphene characterization

3.3.1 Atomic Force Microscopy

Atomic force microscopy is a type of scanning probe microscopy, with nanometric resolution, and is used to obtain topographic images of surfaces [70].

In figure 3.2 is represented the AFM configuration and its components. The AFM probes the sample

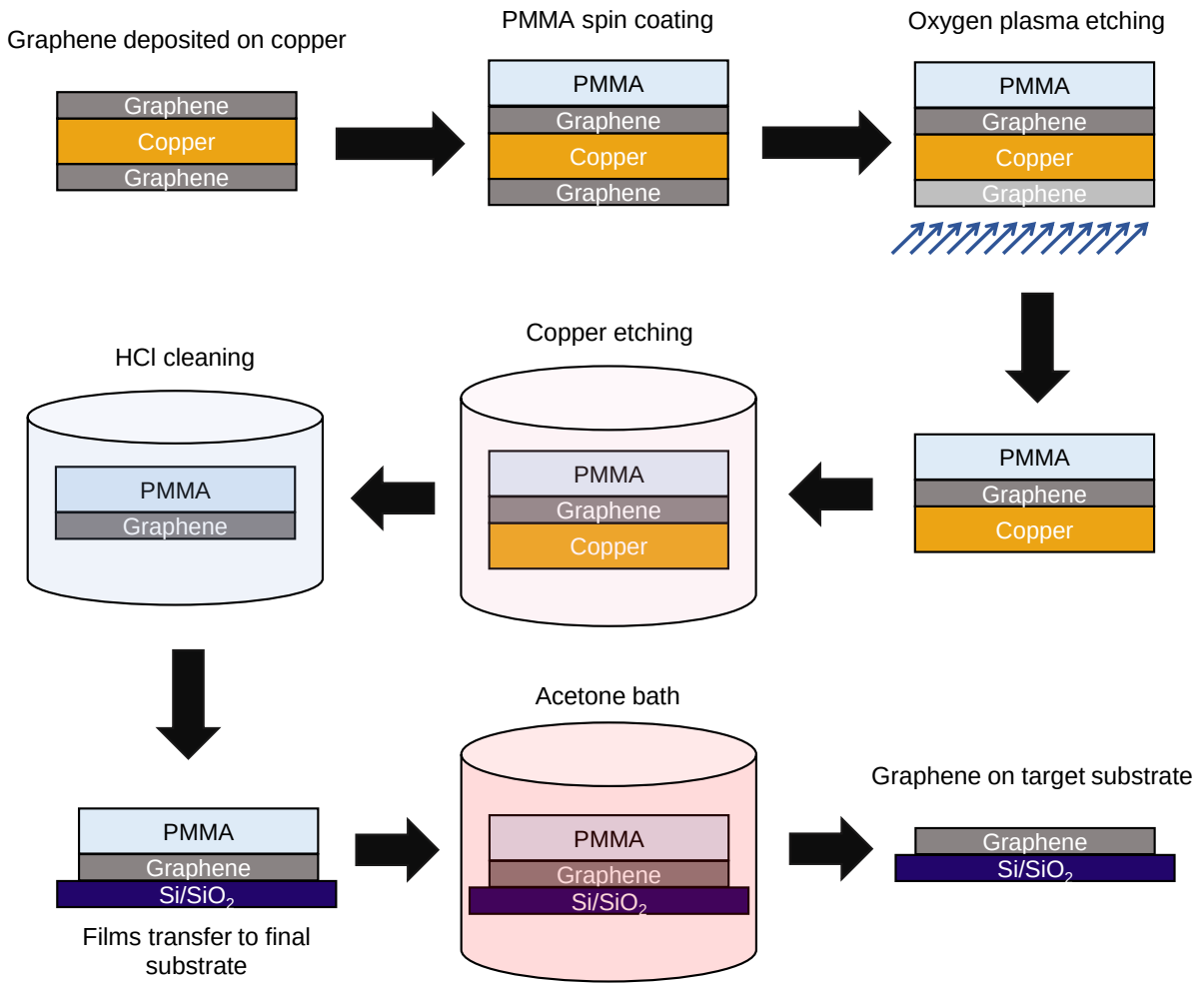

Figure 3.1: Fundamental steps of CVD graphene transfer by the PMMA method.

surface with a nanometric tip which is attached to the end of the cantilever. The cantilver deflects when the tip is brought close to the sample surface, due to the forces (such as Van der Walls or electrostatic forces) caused by tip-surface interactions. The deflection is measured by a photodetector that reflects an incident beam off the top of the cantilever. The direction of the laser beam is altered by changes in cantilever deflection. The topographic images are obtained by scanning the probe tip over the sample surface. Surface features (high and low point of the surface), cause alteration in tip-surface interaction which can be interactions are measured by shifts in frequency, amplitude, phase and height [71].

AFM can be operated in different modes, depending on the tip motion. In the contact mode, the tip is kept in close contact to the surface (around 10 angstroms from the surface) and the interatomic force between surface and cantilever is repulsive. On the other hand in the non-contact mode the tip is kept at a tens to thousands of angstroms from the surface and interatomic force between the cantilever and the surface is attractive. Although in contact mode, the obtained images have higher resolution, the tip is more susceptible of being damaged. A compromise between both modes is the tapping mode, in which

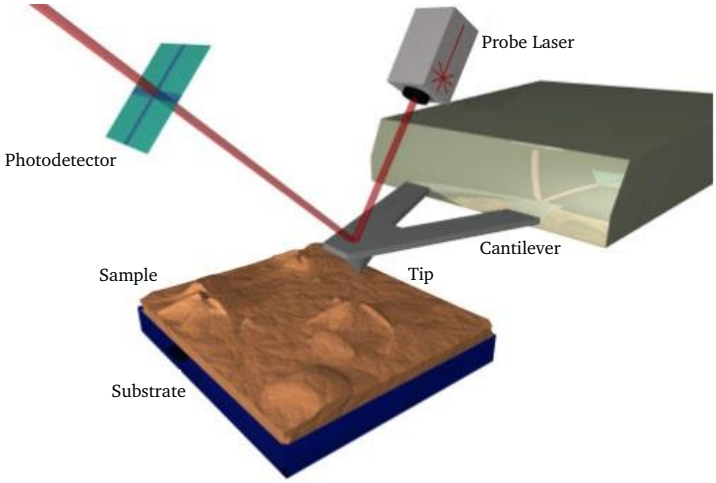

Figure 3.2: AFM basic components. Adapted from [72].

the tip is oscillating up and down [73].

3.3.2 AFM Tapping mode

In tapping mode, also know as the intermittent contact mode, the probe scans the surface by gently tapping the substrate surface. One of the great advantages of this mode is that the tip is not dragged through the surface, avoiding problems caused by friction, adhesion and electrostatic forces. The cantilever is excited to oscillate near its resonance frequency. When the tip is not in contact with the surface, the cantilever oscillates at higher frequencies. When it is brought closer to the surface, and reaches it, the tip-surface interactions cause the cantilever frequency to decrease, as the surface is scanned. The oscillation amplitude is dependent on tip-surface interaction forces. In tapping mode, the image is produced by retrieving the data regarding the reduction in oscillation amplitude. A feedback loop keeps the oscillation amplitude constant, and when an elevated (or lowered area) is scanned, the amplitude is altered since the cantilever has more (or less) space to oscillate [74, 75, 76].

3.3.3 Processing and analysis of an AFM image

In this project, the Nanoscope software was used in image processing and analysis of AFM images. Filters were applied to correct unwanted features fromt the images. Thus, to retrieve information about surface properties of samples, images were analyzed not only to obtain a 2D and 3D image of the scanned surface, but also data about depth and width, roughness, particles, electrochemestry, and more.

Image processing

Since the probe is moved over the surface in a curved motion the obtained AFM images had a bow or a tilt. The *flatten* command was to remove these undesirable features from the scan lines. The software fits each line individually to center data (Oth order) and remove tilt (1st order), or bow (2nd and 3rd order). The software calculated a polynominal equation to fit each line, as described in table 3.1. By subtracting the obtained polynomial to the bow or tilt, each line was flattened [77].

Order	Polynomial	Description
0	$z = a$	Data is centered along each line
1	$z = ax + b$	Data is centered and tilt is removed in each line. Offset and slope are eliminated
2	$z = ax^2 + bx + c$	Data is centered and tilt and bow are removed along each line. A second order equation is calculated to each line, and subtrated from it.
3	$z = ax^3 + bx^2 + cx + d$	Data is centered and tilt and bow are removed along each line. A third order equation is calculated to each line, and subtrated from it.

Table 3.1: Polynomial equation to used to correct the bow, and tilts [77].

The *Plane fit* command was used in image correction, in a similar manner as the *Flatten* command, however in can be used in both XY directions, to correct images with unwanted features.

The *erase* command was used to correct the image. With this function it is possible to replace areas and lines with an interpolation from the adjacent lines.

Each of the obtained images has a scan size of 10μm (area: 100 μm^2) and 2048 samples were obtained per line. 2048 lines were obtained. The resolution of each image is around 5 nm.

Particle analysis

To be able to perform a comparative analysis on the amount of PMMA residues in each sample it was necessary to run the *Particle Analysis* command, which was designed to identify isolated particules or features. Data was sorted based on pixel data height and particles were treated as conjoined pixels below or above a previously set threshold height.

Thus, particles can be sorted by size in a histogram, providing information about particle mean area, total number of particles. The software provides information about the mean, maximum, minimum, and standard deviation in each data set, of the following parameters:

- Total count of particles;
- Density of particles;
- Height of particles;
- Area of particles;
- Diameter of particles.

Roughness analysis

To determine the quality of the transfer, and to be able to measure the amount of irregularities in graphene's surface, such as wrinkles or ruptures, a roughness analysis was performed. With this analysis several roughness parameters can be obtained, from the entire image or from a specific region in the sample surface. Data is obtained using the height of every pixel in the image. The typical roughness parameters obtained are:

- Mean: mean value of the data retrived from the examined section;
- Z range: maximum vertical distance between the lowest and highest points in the examined section, prior to the planefit;
- Surface Area: three-dimensional area of the section;
- Projected surface area: area of the studied section;
- Surface area difference: difference between the projected surface area and the surface area;
- Rq (roughness) : root mean square of height deviations retrieved from the mean image date plane;
- Ra (roughness average): arithmetic average of absolute values of height deviations from the mean plane;
- Rmax: maximum vertical distance between the highest and lowest data points in the image after the plane fit.

Thus, the software retrieves data about peaks and valleys in the image or in a chosen area:

- Peak/Valley count: number of peaks(valleys) above (below) the threshold;
- Max peak height/depth: highest/lowest data point in the image;
- Average maximum height/depth: Average distance between the mean data plane highest/lowest data points.

Chapter 4

Results and discussion

4.1 CVD graphene transfer by the PMMA method

To optimize CVD graphene transfer into a substrate, the effect of modifications in the standard process described in section 3.2.1 and in image 3.1 was studied. Both particle and roughness analysis were carried out, to understand the effect of the modifications in the amount of PMMA residues in the surface and the amount of breaks and wrinkles. Particle analysis and roughness studies were conducted both on the entire AFM images and on $1 \times 1 \mu m^2$ sections of those images. Also, optical microscope images were obtained. The darkest grey area in the images corresponds to transfered graphene and the blue spots/areas correspond to PMMA residues.

4.1.1 Standard PMMA transfer

A study was carried out on a standard PMMA CVD graphene transfer batch, which was obtained by the process described on section 3.2.1 and in image 3.1. AFM and optical microscope images obtained from these batches can be observed in figure 4.1 and 4.2. The success rate (rate of transfers in which the graphene is not visibly damaged) of these transfers is around 50%.

4.1.2 Transfer with additional HCl cleaning steps

A study was carried out on a PMMA CVD graphene transfer batch similar to the standard PMMA transfer, except in the HCl cleaning step. The cleaning steps were altered to 20 min in each beaker: 2 times (20

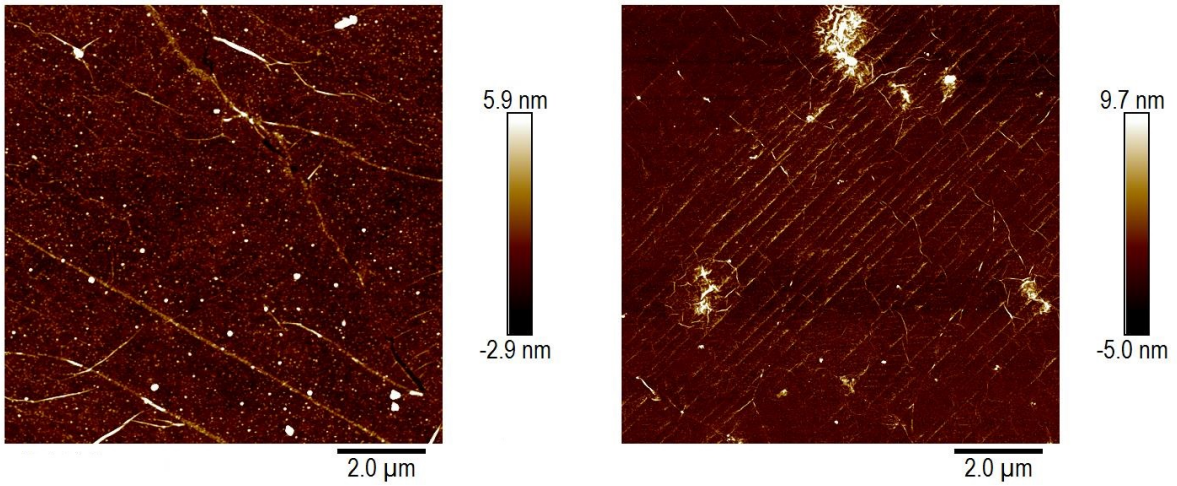

Figure 4.1: AFM images of CVD graphene transfered by the standard PMMA method.

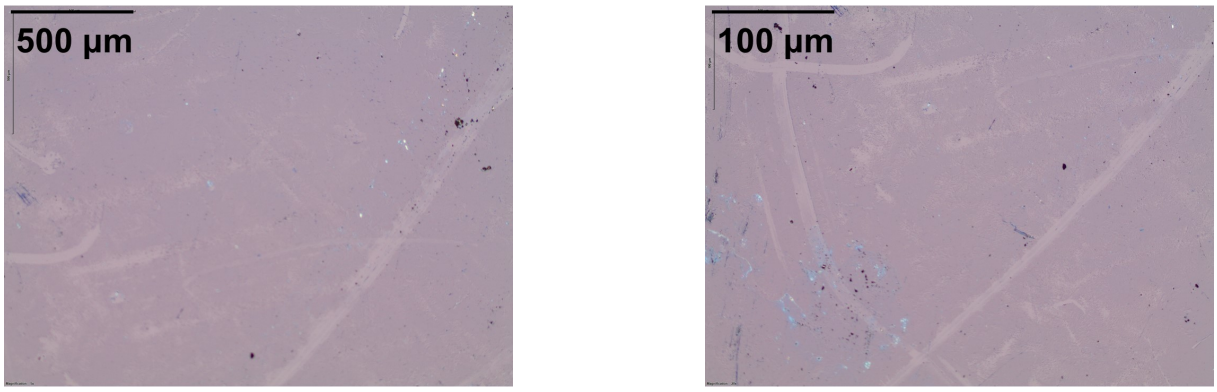

(a) Optical microscope image obtained with magnification 5x.

(b) Optical microscope image obtained with magnification 20x.

Figure 4.2: Optical microscope images of CVD graphene transfered by the standard PMMA method, with different magnifications.

min each time) in DI water and then one time in HCl and finally 3 times in DI water (20 min each time). AFM and optical microscope images obtained from these batches can be observed in figure 4.3 and 4.4. The success rate of these transfers was 30%.

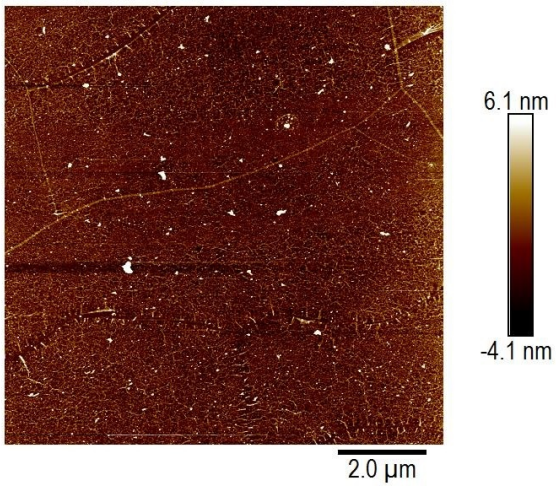

Figure 4.3: AFM images of CVD graphene transfer carried out with modified HCl cleaning step.

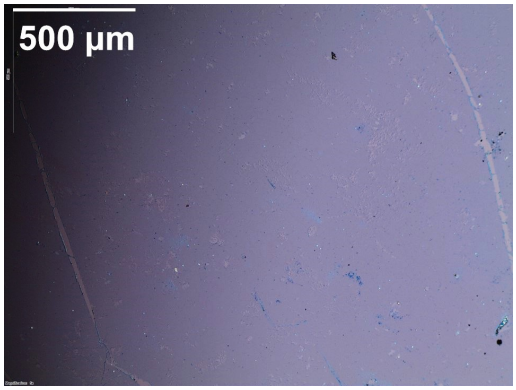

(a) Optical microscope image obtained with magnification 5x.

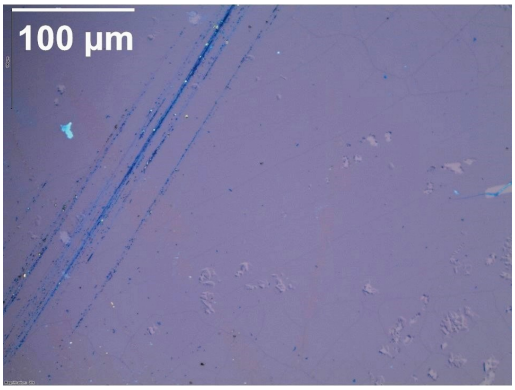

(b) Optical microscope image obtained with magnification 20x.

Figure 4.4: Optical microscope images of CVD graphene transfer carried out with modified HCl cleaning step, with different magnifications.

4.1.3 Double PMMA layer transfer

A study was carried out on a PMMA CVD graphene transfer batch similar to the standard PMMA transfer, except that, after the first A6 950 K PMMA layer was spin coated (and the polymer was cured in air for 10 minutes), a droplet of A3 950K PMMA was added and cured in air for 2 hours. AFM and optical microscope images obtained from these batches can be seen in figure 4.5 and 4.6. The success rate of these transfers was 30%.

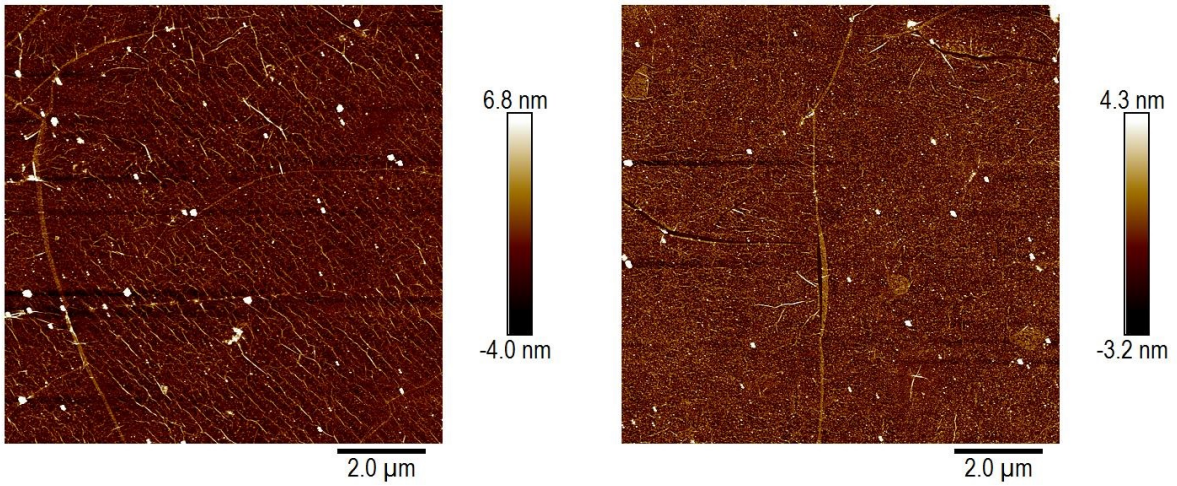

Figure 4.5: AFM images of CVD graphene transfer carried out with a double PMMA layer.

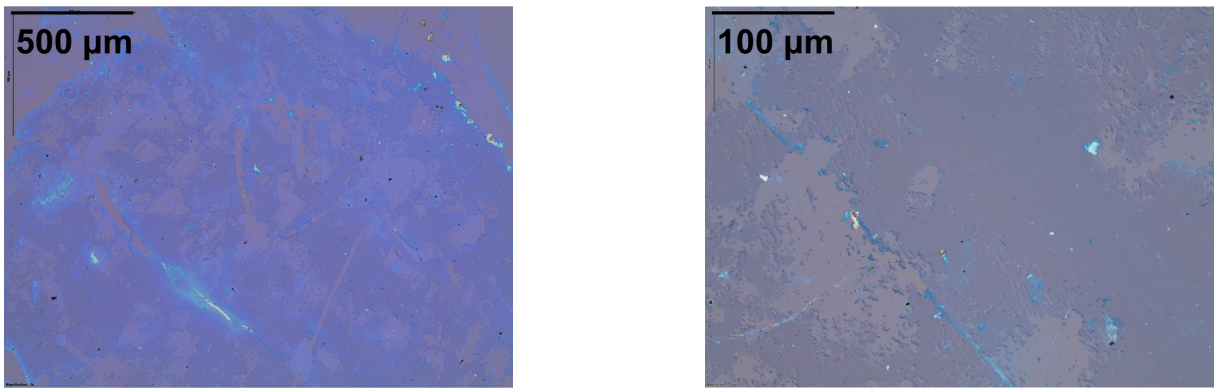

(a) Optical microscope image obtained with magnification 5x.

(b) Optical microscope image obtained with magnification 20x.

Figure 4.6: Optical microscope images of CVD graphene transfer carried out with a double PMMA layer, with different magnifications.

4.1.4 Addition of a baking step after spin coating

A study was carried out on a PMMA CVD graphene transfer batch similar to the standard PMMA transfer, except that, after spin coating, the samples graphene/PMMA films were baked for 5 min at 80°C and then at 130°C for 20 min. AFM and optical microscope images obtained from these batches can be observed in figure 4.7 and 4.8. The success rate of these transfers was 90%.

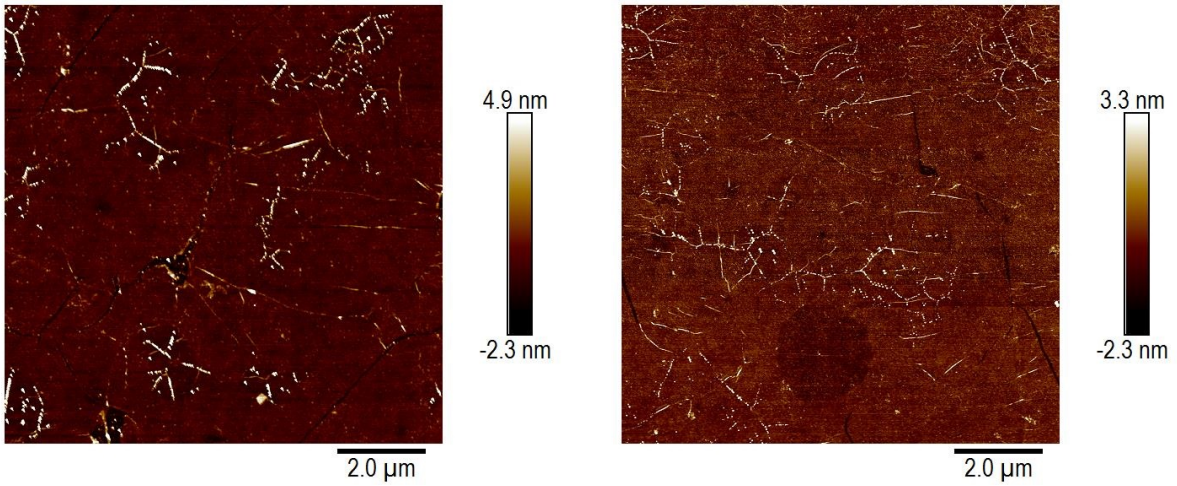

Figure 4.7: AFM images of CVD graphene transfer with an additional baking step after spin coating.

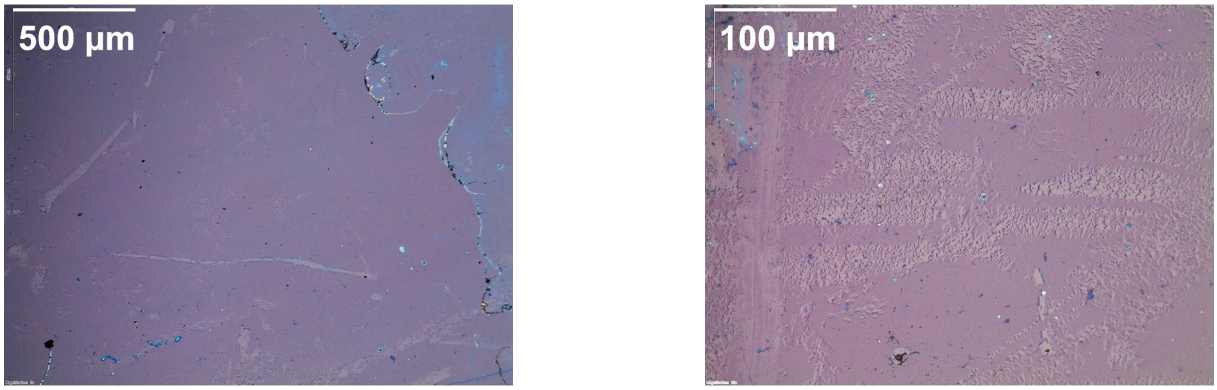

(a) Optical microscope image obtained with magnification 5x.

(b) Optical microscope image obtained with magnification 20x.

Figure 4.8: Optical microscope images of CVD graphene transfer carried outwith an additional baking step after spin coating, with different magnifications.

4.1.5 Addition of a baking step after transfer to substrate

A study was carried out on a PMMA CVD graphene transfer batch similar to the standard PMMA transfer, except that, after HCl cleaning and transfer of PMMA/graphene/copper/substrate, the samples were baked for 5 min at 80°C and then 20 min at 130°C. AFM and optical microscope images obtained from these batches can be seen in figure 4.9 and 4.10. The success rate of these transfers was 90%.

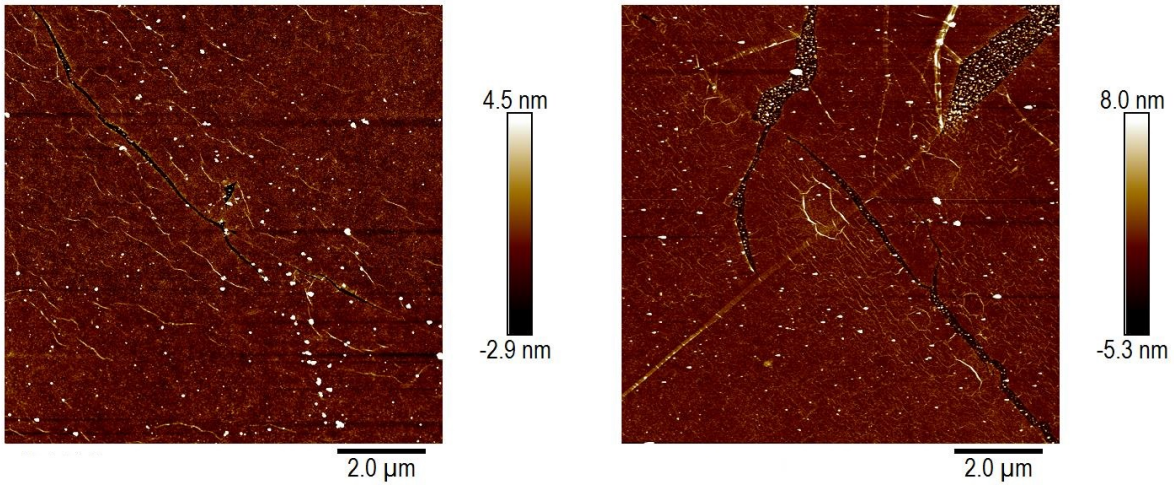

Figure 4.9: AFM images of CVD graphene transfer with a baking step after transfer to substrate.

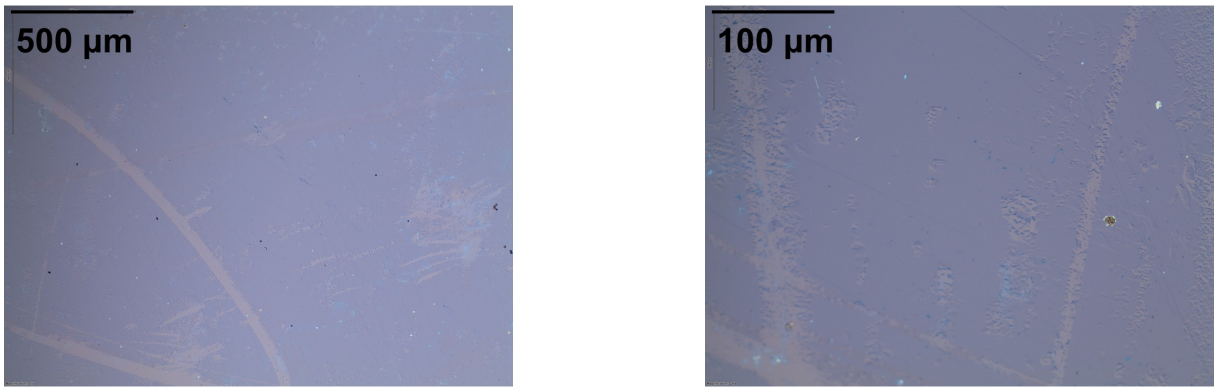

(a) Optical microscope image obtained with magnification 5x.

(b) Optical microscope image obtained with magnification 20x.

Figure 4.10: Optical microscope images of CVD graphene transfer with a baking step after transfer to substrate, with different magnifications.

4.1.6 Addition of a baking step after transfer to substrate and annealing

A study was carried out on a PMMA CVD graphene transfer batch, similar to the standard PMMA transfer, except that, after HCl cleaning and transfer of PMMA/graphene/copper/substrate, the samples were baked for 5 min at 80°C and then 20 min at 130°C. Thus, after the acetone bath the samples were annealed for 2 hours at 500°C with a forming gas flow of hydrogen and argon. AFM and optical microscope images obtained from these batches can be seen in figure 4.11 and 4.12. The success rate of these transfers was 90%.

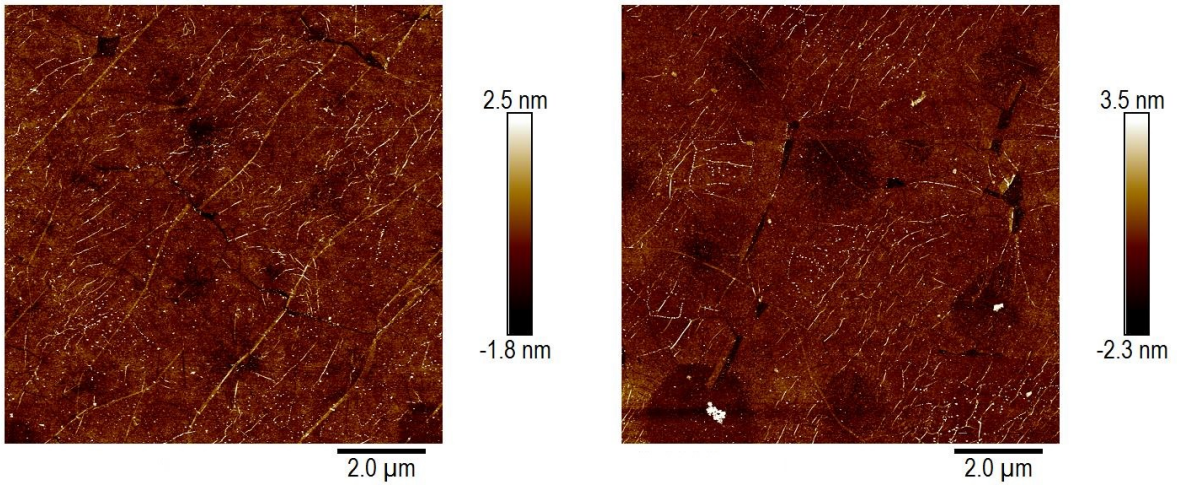

Figure 4.11: AFM images of CVD graphene transfer with a baking step after transfer to substrate and annealing after acetone bath.

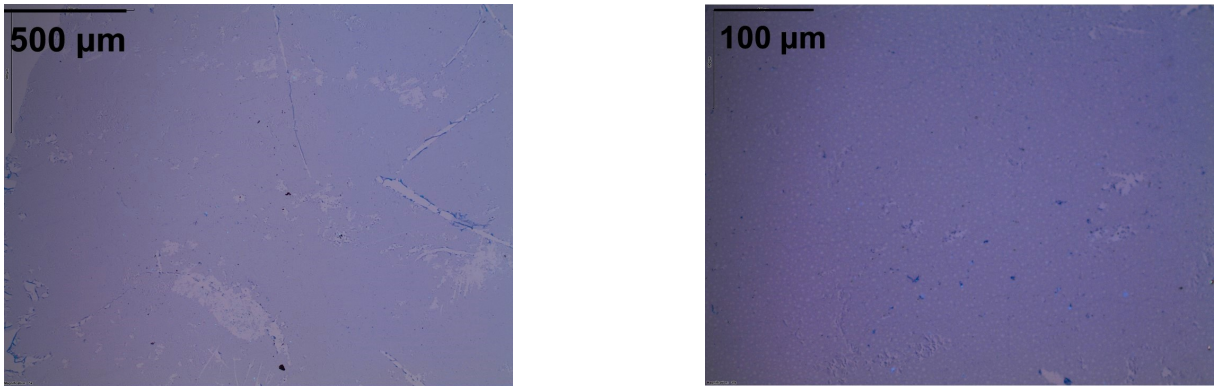

(a) Optical microscope image obtained with magnification 5x.

(b) Optical microscope image obtained with magnification 20x.

Figure 4.12: Optical microscope images of CVD graphene transfer with a baking step after transfer to substrate and annealing after acetone bath, with different magnifications.

4.1.7 Double layer transfer and annealing

A study was carried out on a PMMA CVD graphene transfer batch similar to the standard PMMA transfer, except that, after the first A6 950 K PMMA layer was spin coated (and the polymer was cured in air for 10 minutes), a droplet of A3 950K PMMA was added and cured in air for 2 hours. Thus, after the acetone bath the samples were annealed for 2 hours at 500^{o}C with a forming gas flow of hydrogen and argon. AFM and optical microscope images obtained from these batches can be seen in figure 4.13 and 4.14. The success rate of these transfers was 30%.

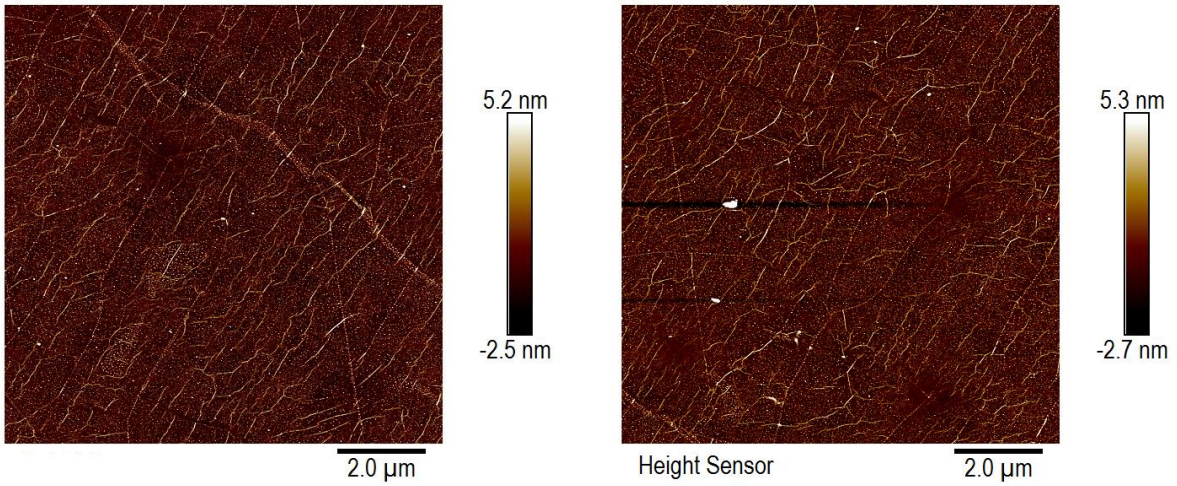

Figure 4.13: AFM images of CVD graphene transfer carried out with a double PMMA layer and annealing after acetone bath.

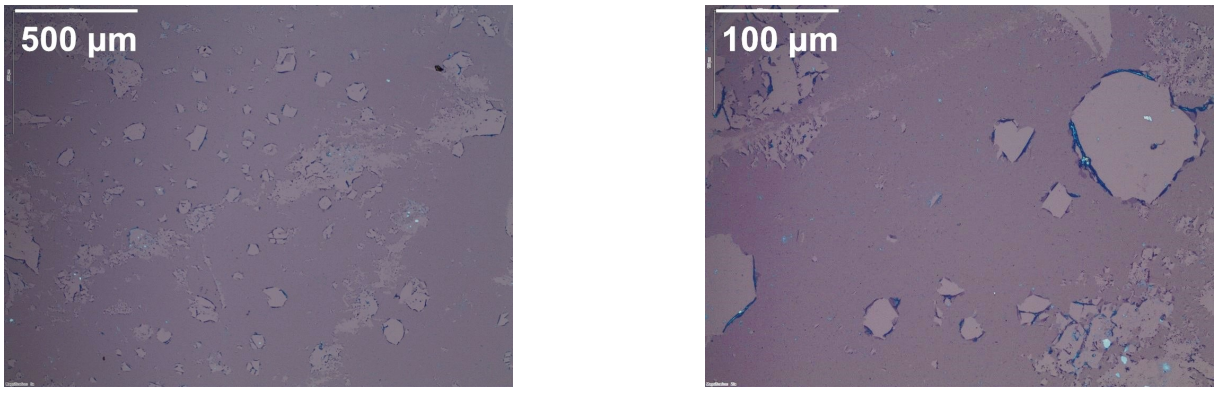

(a) Optical microscope image obtained with magnification 5x.

(b) Optical microscope image obtained with magnification 20x.

Figure 4.14: Optical microscope images of CVD graphene transfer carried out with a double PMMA layer and annealing after acetone bath, with different magnifications.

4.2 Particle and roughness analysis

4.2.1 AFM and optical images inspection

From the images in figures 4.1 and 4.2, the common irregularities associated with CVD graphene transfers can be seen. The white dots shown in the left AFM image, are PMMA residues. The white lines correspond to wrinkles, and can be observed in both images. In the optical microscope images, several tears in the graphene membrane can be observed. Images obtained for the additional HCl cleaning steps, shown in figures 4.3 and 4.4, show a reduction in the amount of wrinkles, PMMA residues and breaks in the graphene membrane. On the other hand, addition of a second PMMA layer deteriorated

graphene quality by increasing the amount of breaks and tears, as shown in image 4.6. In the images from figures 4.7 and 4.8, that correspond to the experiments with an additional baking step after spin coating, the presence of wrinkles and breaks in the graphene membrane can be observed, however in a smaller quantity, if compared with the images obtained for the standard transfer. Also, it is visible a reduction in the amount of PMMA residues. Addition of a baking step after the transfer lead to rupturing of the graphene membrane, as shown in the images from figures 4.9 and 4.10. It can be observed an accumulation of PMMA residues around ruptured area. Comparing images from figures 4.13 and 4.14, it can be observed that addition of an annealing step after the acetone bath lead to a reduction of PMMA residues in the sample surface.

4.2.2 Particle analysis

An analysis was conducted on the particles present in the AFM images, to study the effect of the implemented modifications on PMMA residue density. Particle density for each AFM image was retrieved, as shown in the tables from Appendix A. Also, particle density average and standard deviation were obtained. In table 4.1 can be seen the particle density average for each of the modifications on the standard process. Also, with the box plots shown in figure 4.15, data distribution and the reproducibility of the conducted experiments can be assessed.

	Particle density average ($/\mu m^2$)	**Count**
Standard	1,99	5
Extra HCl cleaning	0,44	1
Double layer	1,75	6
Baking after spin coating	1,07	6
Baking after transfer to substrate	0,71	5
Baking after transfer to substrate and annealing	0,23	5
Double layer and annealing	0,58	5

Table 4.1: Average values obtained for particle density of each image and the number of images used to retrieve the data.

Compared with the standard transfer, the modified HCl cleaning decreased the average particle density by 78%; the double layer transfer by 14%; the transfer with baking after spin coating by 46% and the baking after transfer to substrate by 65 %. Also, after annealing the samples, the particle density in the transfers with baking step after transfer to substrate, decreased by 78% and, in the double layer transfers, it was reduced by 67%.

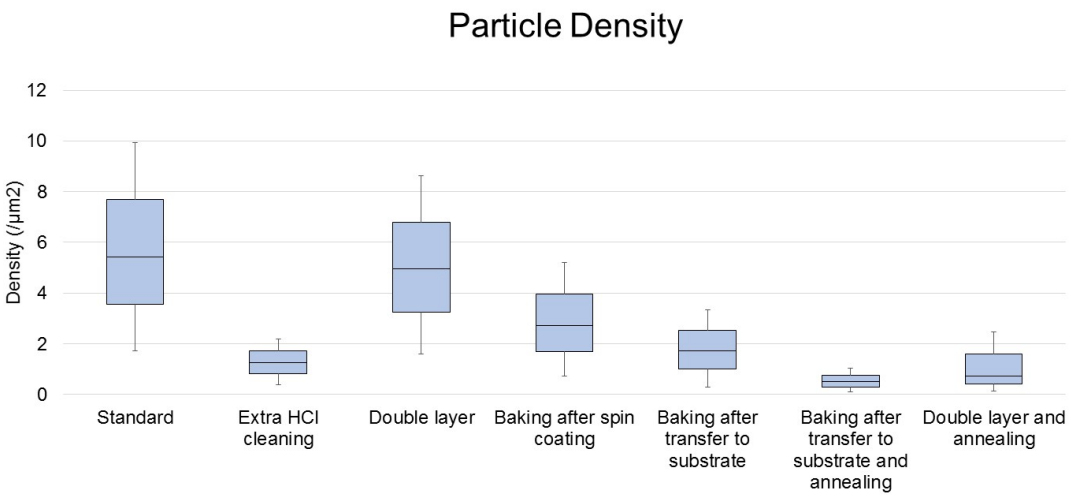

Figure 4.15: Particle density measurements in AFM images obtained with the standard PMMA transfer and with modifications.

Analyzing the plot from figure 4.15 and the figures obtained for particle density average, it can be verified that both the standard PMMA and the double layer transfer generate the images with the highest density of particles, and produced the most disperse data. Although, with the double layer transfer, particle density average has been reduced by 14%, the amount of micrometer sized tears and ripples is evident, as shown in image 4.14. Also, since the data retrieved is quite disperse, the results of this experiments are less reproducible, if compared to the experiments carried with other modifications. An increase in PMMA particle density would be expected with the addition of another polymer layer to the copper/graphene/PMMA stack. Baking the films after spin coating also caused a reduction of PMMA residue density since it lead to hardening of the PMMA layer, decreasing the probability of it being destroyed during sample handling while it was still not dry. An additional baking step after the transfer to the substrate lead to a decrease on average particle density. However, it should be remarked that PMMA residues tend to accumulate in irregular areas, suck as breaks or tears of the graphene membrane. For this reason, increasing the duration of HCl cleaning steps lead to a significant decrease in residue density. An efficient removal of wet etchant lead to an improved contact between graphene and substrate, reducing the probability of rupturing the graphene. Annealing the graphene caused the disintegration of PMMA particles due to exposure to high temperatures, leading to a significant decrease in particle density.

4.2.3 Roughness Analysis

A roughness analysis was conducted on the AFM images to study the effect of the implemented modifications on PMMA residue density. Roughness parameters for each AFM image, and for $1 \times 1\mu m^2$

sections were retrieved, as shown in the tables from Appendix A. It was obtained the average and standard deviation for both image and section maximum vertical range (Z range), roughness (Rq) and roughness average (Ra). The average of the roughness parameters, for each of of the modifications is shown in table 4.2. Also, with the box plots shown in figures 4.16, 4.17, 4.18, 4.19, 4.20 and 4.21, data distribution and the reproducibility of the conducted experiments can be assessed.

	Image				**Section**			
	Z range (nm)	Rq (nm)	Ra (nm)	Count	Z range (nm)	Rq (nm)	Ra (nm)	Count
Standard	107,27	3,24	1,79	3	14,50	1,60	1,20	15
Extra HCl cleaning	58,80	1,45	0,84	1	9,18	0,90	0,70	5
Double layer	80,90	2,59	1,20	6	12,34	1,03	0,76	26
Baking after spin coating	25,97	0,91	0,50	6	5,86	0,44	0,31	24
Baking after transfer to substrate	108,42	2,46	0,84	5	9,15	1,51	0,69	20
Baking after transfer to substrate and annealing	29,50	0,78	0,47	6	4,48	0,42	0,34	26
Double layer and annealing	58,44	1,46	0,87	5	8,90	0,92	0,67	24

Table 4.2: Average values obtained for both image and section maximum vertical range (Z range), roughness (Rq) and roughness average (Ra). Also, the number of samples used in each experiment of this analysis is shown. These values were obtained from the tables shown in appendix A.

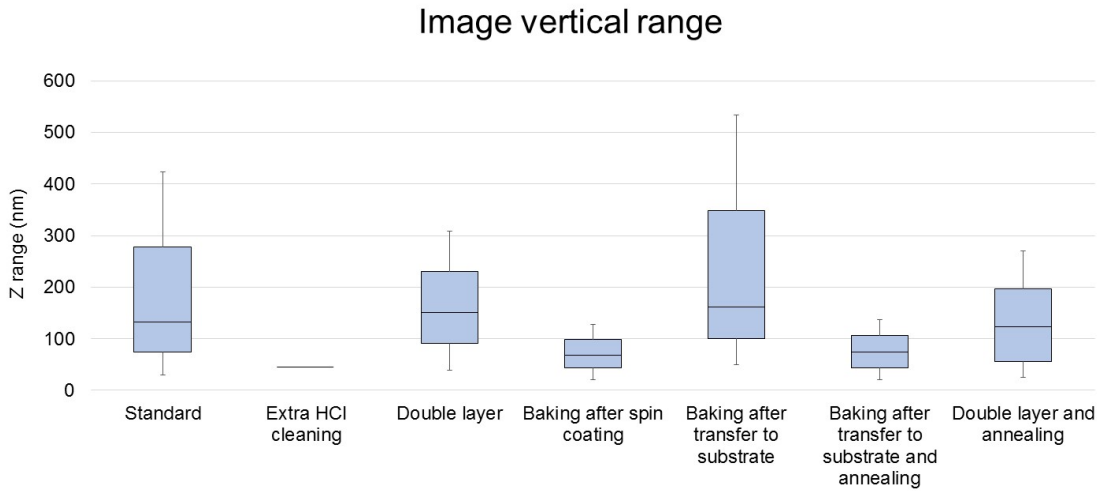

Figure 4.16: Maximum vertical range measurements in AFM images obtained with the standard PMMA transfer and the modifications.

Compared with the standard transfer, the modified HCl cleaning decreased image average maximum

vertical range by 45%; the double layer transfer by 25%; the transfer with baking after spin coating by 75% and the baking after transfer had no effect on the vertical range. Also, after annealing the samples, the maximum vertical range in the transfers with baking step after transfer to substrate decreased by 73% and in the double layer transfers it was reduced by 77%.

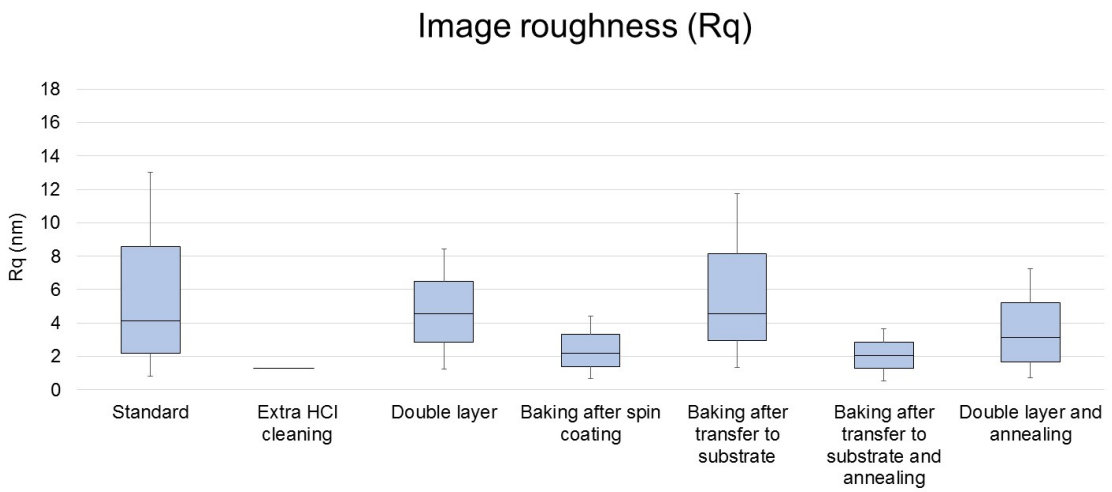

Figure 4.17: Roughness (Rq) measurements in AFM images obtained with the standard PMMA transfer and the modifications.

Compared with the standard transfer, the modified HCl cleaning decreased the average image roughness (Rq) by 55%; the double layer transfer by 20%; the transfer with baking after spin coating by 70% and the baking after transfer by 73%. Also, after annealing the samples, the maximum vertical range in the transfers with baking step after transfer to substrate decreased by 70% and in the double layer transfers it was reduced by 44%.

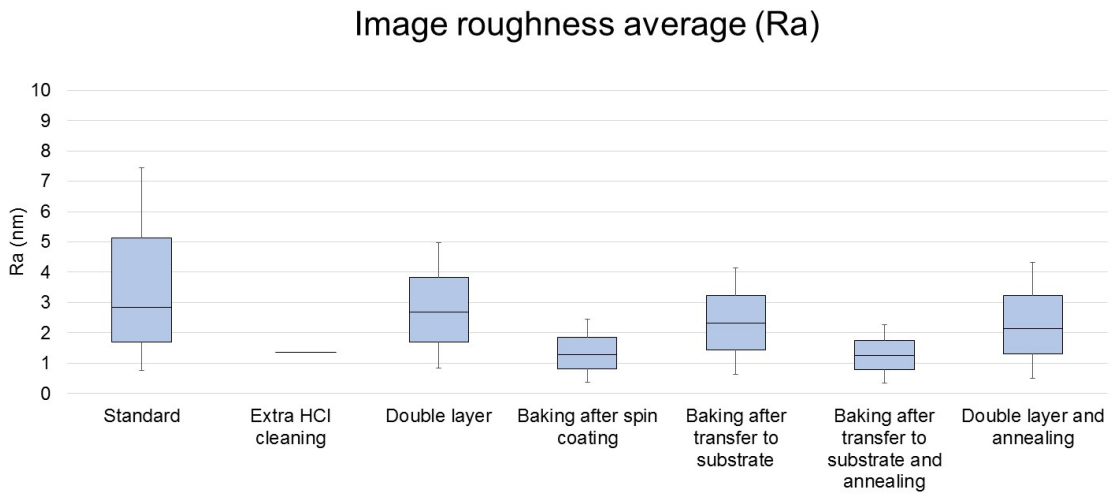

Figure 4.18: Roughness average (Ra) measurements in AFM images obtained with the standard PMMA transfer and the modifications.

Compared with the standard transfer, the modified HCl cleaning decreased the average image roughness (Ra) 53%; the double layer transfer by 34%; the transfer with baking after spin coating by 25% and the baking after transfer by 72%. Also, after annealing the samples, the maximum vertical range in the transfers with baking step after transfer to substrate decreased by 45% and in the double layer transfers it was reduced by 52%.

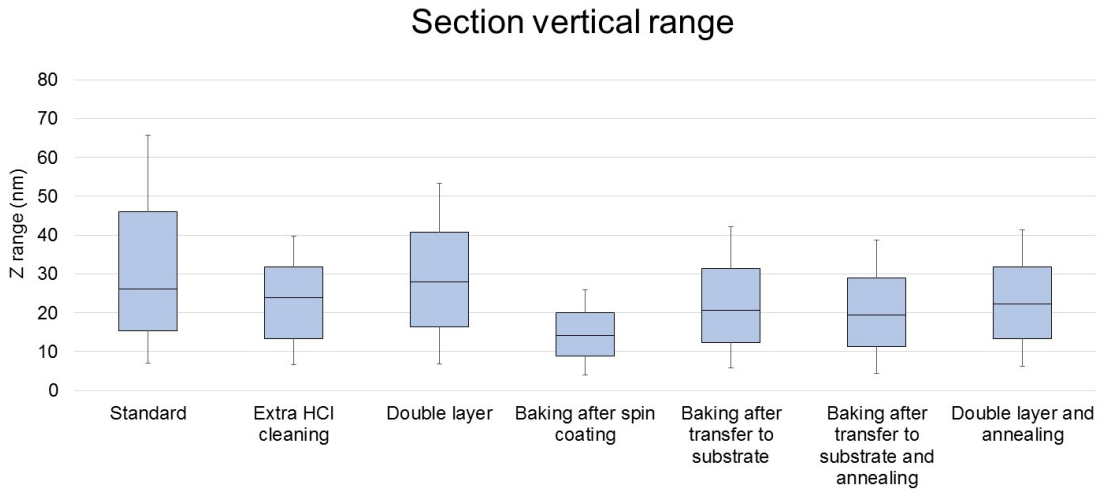

Figure 4.19: Maximum vertical range measurements in $1 \times 1\mu m^2$sections of AFM images obtained with the standard PMMA transfer and the modifications.

Compared with the standard transfer, the modified HCl cleaning decreased the section average maximum vertical range by 37%; the double layer transfer by 15%; the transfer with baking after spin coating by 60% and the baking after transfer by 37%. Also, after annealing the samples, the maximum vertical range in the transfers with baking step after transfer to substrate decreased by 48% and in the double layer transfers it was reduced by 28%.

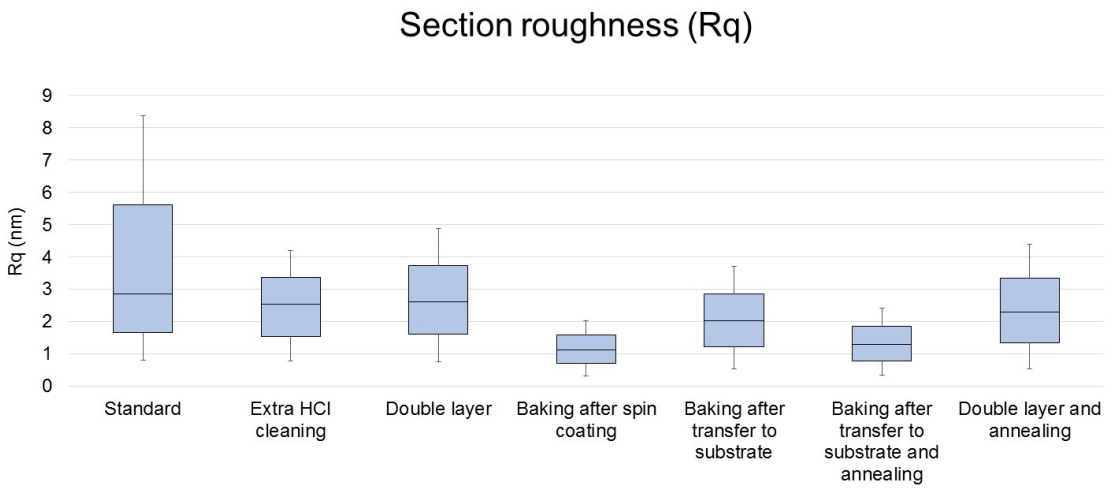

Figure 4.20: Roughness (Rq) measurements in $1 \times 1\mu m^2$sections of AFM images obtained with the standard PMMA transfer and the modifications.

Compared with the standard transfer, the modified HCl cleaning decreased the section average image roughness (Rq) 44%; the double layer transfer by 35%; the transfer with baking after spin coating by 73% and the baking after transfer by 5%. Also, after annealing the samples, the maximum vertical range in the transfers with baking step after transfer to substrate decreased by 73% and in the double layer transfers it was reduced by 48%

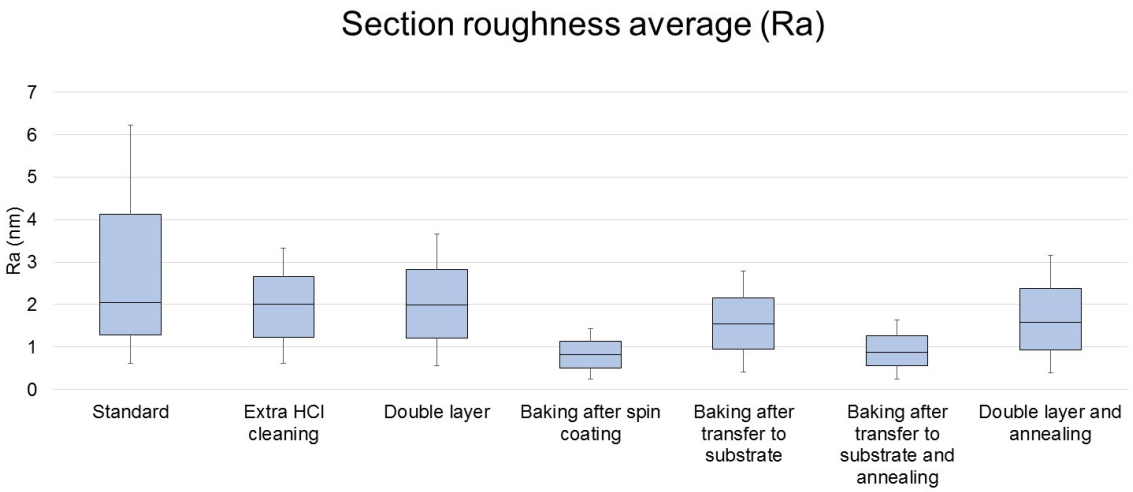

Figure 4.21: Roughness average (Ra) measurements in $1 \times 1 \mu m^2$sections of AFM images obtained with the standard PMMA transfer and the modifications.

Compared with the standard transfer, the modified HCl cleaning decreased the section average image roughness (Ra) 42%; the double layer transfer by 37%; the transfer with baking after spin coating by 75% and the baking after transfer by 40%. Also, after annealing the samples, the maximum vertical range in the transfers with baking step after transfer to substrate decreased by 50% and in the double layer transfers, it was reduced by 12%.

To further understand the effect of the implemented modifications in roughness parameters, data from the entire images (figures: 4.16, 4.17, 4.18) and from sections without PMMA residues or major irregularities (figures: 4.19, 4.20 and 4.21) was retrieved, to assess data uniformity. Data uniformity is altered by irregularities on the sample surface. The data obtained for the entire image varied in a wider range, but is consistent with the values obtained for the selected sections. An experiment with extra cleaning steps was carried out with the goal of improving the cleanliness of the graphene, by removing copper etchant particles that remained attached to the graphene, promoting adhesion of the graphene to the substrate. Although in this experiment the roughness parameters are improved (section parameter improvement varies from 37% to 44%), the success rate was 20% lower than in the standard transfer, because graphene remained in the HCl bath for 20 min, which lead to graphene degradation. Thus, longer DI water cleaning steps lead to improvements. The double layer experiment was carried with

the goal of the second PMMA layer diluting the first layer, relaxing it and enhancing contact between graphene and substrate. Although the roughness parameters improve (section parameter improvement varies from 15% to 37%), the success rate was 20% lower than in the standard PMMA transfer.Also, the optical microscope images from figures 4.6, show increased breaking and rippling of the graphene membrane as shown in the images of figure 4.14. To harden the PMMA and provide a more efficient graphene support, the PMMA was baked after spin coating. This modification lead to a 40% increase in the success rate and to an 60% to 75% improvement in the section roughness parameters. Also, an experiment was conducted in which the graphene/PMMA films were baked after being transfered, to evaporate any trapped water between graphene and the substrate. If graphene is not properly attached to the substrate, those regions will break, causing tears and ripples when the PMMA is removed. This modification showed an 40% success rate increase and improvements from 5 % to 40 % in section roughness parameters. AFM images from figure 4.9 and an elevated dispersion of the values obtained for image parameters, as shown in the plots from figures 4.16 and 4.17, demonstrate that, despite the improvements on roughness in the section paramenters, which correspond to areas where the graphene appeared intact, this modification lead to breaking of the membrane. Annealing the samples, produced overall improvements, specially on image roughness parameters due to PMMA residues removal, for both experiments conducted.

Chapter 5

Conclusions

5.1 Achievements

The effect of modifications to the CVD graphene transfer by the PMMA method was studied. Optical and AFM images were retrieved to quantify the effects of the modifications implemented. Particle density and roughness parameters were obtained and a comparative analysis of the data was performed.

Longer HCl cleaning steps enhance the removal of copper etchant residues of the graphene surface. This modification lead to a decrease on residue accumulation and roughness. Optical microscope images showed improvements in rupturing and tearing of graphene membrane. However, only DI water cleaning steps seemed to improve the transfer quality.

Also, the effect of adding a second PMMA layer was studied. Optical images show that the amount of breaking and tearing is significant. However, improvements on PMMA residue accumulation and on roughness parameters were achieved.

Furthermore, an experiment with an additional baking step after spin coating was carried, which showed a significant increase in success rate, section roughness parameters and in particle density. Optical microscope images also showed the formation of wrinkles. An additional baking step was included after the graphene/PMMA films transfer to the substrate. This modification lead to improvements in particle density section roughness parameters and success rate.

Annealing enhances the removal of PMMA residues in the graphene membrane, leading to improvements on particle density and roughness parameters.

5.2 Future Work

To improve CVD graphene transfer by the PMMA method, longer DI water cleaning steps should be included in all the transfers, to prevent accumulation of copper etchant residues between the graphene and the substrate. Addition of baking steps after transferring the graphene/PMMA stack to the substrate will increase the time efficiency of the transfer process, since the 2 hours drying step, between the stack transfer and acetone bath, would be eliminated. Optimization of this baking step should be considered, in order to decrease rupturing of the graphene membrane.

To use CVD graphene transfered by the PMMA method, the effect of high temperature annealing on electronic properties of graphene should be further studied. Experiments on the efficiency of PMMA removal residues at lower temperatures should also be conducted.

A polymer-free transfer method would further decrease the amount of transferring steps in the process. Performing a transfer with no polymer would eliminate the irregularities caused by the use of a polymer support.

Bibliography

[1] J. Shendure and H. Ji, “Next-generation DNA sequencing,” *Nature Biotechnology*, vol. 26, no. 10, pp. 1135–1145, 2008.

[2] F. Sanger, S. Nicklen, and a. R. Coulson, “DNA sequencing with chain-terminating inhibitors.,” *Proceedings of the National Academy of Sciences of the United States of America*, vol. 74, no. 12, pp. 5463–5467, 1977.

[3] O. Troyanskaya, M. Cantor, G. Sherlock, P. Brown, T. Hastie, R. Tibshirani, D. Botstein, and R. B. Altman, “Missing value estimation methods for DNA microarrays,” *Bioinformatics*, vol. 17, no. 6, pp. 520–525, 2001.

[4] M. J. Heller, “DNA Microarray Technology: Devices, Systems, and Applications,” *Annual Review of Biomedical Engineering*, vol. 4, no. 1, pp. 129–153, 2002.

[5] A. Han, M. Creus, G. Schu, N. F. D. Rooij, and U. Staufer, “Label-Free Detection of Single Protein Molecules and Protein-Protein Interactions Using Synthetic Nanopores,” *Analytical Chemestry*, vol. 80, no. 12, pp. 4651–4658, 2008.

[6] L.-Q. Gu and J. W. Shim, “Single molecule sensing by nanopores and nanopore devices,” *Analyst*, vol. 135, pp. 441–451, 2010.

[7] C. J. Russo and J. A. Golovchenko, “Atom-by-atom nucleation and growth of graphene nanopores,” *Proceedings of the National Academy of Sciences*, vol. 109, no. 16, pp. 5953–5957, 2012.

[8] M. Wanunu, “Nanopores : A journey towards DNA sequencing,” *Physics of Life Reviews*, vol. 9, no. 2, pp. 125–158, 2012.

[9] D. H. Stoloff and M. Wanunu, “Recent trends in nanopores for biotechnology,” *Current Opinion in Biotechnology*, vol. 24, no. 4, pp. 699 – 704, 2013.

[10] B. M. Venkatesan and R. Bashir, “Nanopore sensors for nucleic acid analysis,” *Nature Nanotechnology*, vol. 6, no. 10, pp. 615–624, 2011.

[11] L. Ma and S. L. Cockroft, “Biological nanopores for single-molecule biophysics,” *ChemBioChem*, vol. 11, no. 1, pp. 25–34, 2010.

[12] D. Stoddart, A. J. Heron, E. Mikhailova, G. Maglia, and H. Bayley, “Single-nucleotide discrimination in immobilized DNA oligonucleotides with a biological nanopore,” *Proceedings of the National Academy of Sciences*, vol. 106, no. 19, pp. 7702–7707, 2009.

[13] G. F. Schneider and C. Dekker, “DNA sequencing with nanopores,” *Nature Publishing Group*, vol. 30, no. 4, pp. 326–328, 2012.

[14] B. N. Miles, A. P. Ivanov, K. A. Wilson, F. Dogan, D. Japrung, and J. B. Edel, “Single molecule sensing with solid-state nanopores: novel materials, methods, and applications,” *Chemical Society Reviews*, vol. 42, pp. 15–28, 2013.

[15] G. F. Schneider, S. W. Kowalczyk, V. E. Calado, G. Pandraud, H. W. Zandbergen, L. M. K. Vandersypen, and C. Dekker, “DNA Translocation through Graphene Nanopores,” *Nano Letters*, vol. 10, no. 8, pp. 3163–3167, 2010.

[16] A. K. Geim and K. S. Novoselov, “The rise of graphene,” *Nature Materials*, vol. 6, no. 3, pp. 183–191, 2007.

[17] D. C. Elias, R. R. Nair, T. M. G. Mohiuddin, S. V. Morozov, P. Blake, M. P. Halsall, A. C. Ferrari, D. W. Boukhvalov, M. I. Katsnelson, A. K. Geim, and K. S. Novoselov, “Control of Graphene’s Properties by Reversible Hydrogenation: Evidence for Graphane,” *Science*, vol. 323, no. 5914, pp. 610–613, 2009.

[18] X. Wang, X. Li, L. Zhang, Y. Yoon, P. K. Weber, H. Wang, J. Guo, and H. Dai, “N-Doping of Graphene Through Electrothermal Reactions with Ammonia,” *Science*, vol. 324, no. 5928, pp. 768–771, 2009.

[19] C. Lee, X. Wei, J. W. Kysar, and J. Hone, “Measurement of the Elastic Properties and Intrinsic Strength of Monolayer Graphene,” *Science*, vol. 321, no. 5887, pp. 385–388, 2008.

[20] J. S. Bunch, S. S. Verbridge, J. S. Alden, A. M. van der Zande, J. M. Parpia, H. G. Craighead, and P. L. McEuen, “Impermeable Atomic Membranes from Graphene Sheets,” *Nano Letters*, vol. 8, no. 8, pp. 2458–2462, 2008.

[21] H. J. Jeong, H. Y. Kim, S. Y. Jeong, J. T. Han, K. J. Baeg, J. Y. Hwang, and G. W. Lee, “Improved transfer of chemical-vapor-deposited graphene through modification of intermolecular interactions and solubility of poly(methylmethacrylate) layers,” *Carbon*, vol. 66, pp. 612–618, 2014.

[22] D. B. Wells, M. Belkin, J. Comer, and A. Aksimentiev, “Assessing Graphene Nanopores for Sequencing DNA,” *Nano Letters*, vol. 12, no. 8, pp. 4117–4123, 2012.

[23] K. S. Novoselov, A. K. Geim, S. V. Morozov, D. Jiang, Y. Zhang, S. V. Dubonos, I. V. Grigorieva, and A. A. Firsov, “Electric Field Effect in Atomically Thin Carbon Films,” *Science*, vol. 306, no. 5696, pp. 666–669, 2004.

[24] K. S. Novoselov, D. Jiang, F. Schedin, T. J. Booth, V. V. Khotkevich, S. V. Morozov, and A. K. Geim, “Two-dimensional atomic crystals,” *Proceedings of the National Academy of Sciences of the United States of America*, vol. 102, no. 30, pp. 10451–10453, 2005.

[25] K. S. Novoselov, A. K. Geim, S. V. Morozov, D. Jiang, M. I. Katsnelson, I. V. Grigorieva, S. V. Dubonos, and A. A. Firsov, “Two-dimensional gas of massless Dirac fermions in graphene,” *Nature*, vol. 438, no. 7065, pp. 197–200, 2005.

[26] A. N. Obraztsov, “Chemical vapour deposition: Making graphene on a large scale,” *Nature Nanotechnology*, vol. 4, no. 4, pp. 212–213, 2009.

[27] J. Kong, A. M. Cassell, and H. Dai, “Chemical vapor deposition of methane for single-walled carbon nanotubes,” *Chemical Physics Letters*, vol. 292, no. 4–6, pp. 567 – 574, 1998.

[28] Y. C. Shin, M. S. Dresselhaus, and J. Kong, *Carbon Nanotubes and Graphene*. Elsevier, 2014.

[29] A. Reina, X. Jia, J. Ho, D. Nezich, H. Son, V. Bulovic, M. S. Dresselhaus, and J. Kong, “Large Area, Few-Layer Graphene Films on Arbitrary Substrates by Chemical Vapor Deposition,” *Nano Letters*, vol. 9, no. 1, pp. 30–35, 2009.

[30] A. Reina, S. Thiele, X. Jia, S. Bhaviripudi, M. Dresselhaus, J. Schaefer, and J. Kong, “Growth of large-area single- and Bi-layer graphene by controlled carbon precipitation on polycrystalline Ni surfaces,” *Nano Research*, vol. 2, no. 6, pp. 509–516, 2009.

[31] N. Obraztsov, E. Obraztsova, V. Tyurnina, and A. Zolotukhin, “Chemical vapor deposition of thin graphite films of nanometer thickness,” *Carbon*, vol. 45, no. 10, pp. 2017–2021, 2007.

[32] G. Varhegyi, M. J. A. Jr., E. Jakab, and P. Szabo, “Kinetic modeling of biomass pyrolysis,” *Journal of Analytical and Applied Pyrolysis*, vol. 42, no. 1, pp. 73 – 87, 1997.

[33] K. S. Kim, Y. Zhao, H. Jang, S. Y. Lee, J. M. Kim, K. S. Kim, J.-H. Ahn, P. Kim, J.-Y. Choi, and B. H. Hong, “Large-scale pattern growth of graphene films for stretchable transparent electrodes,” *Nature*, vol. 457, no. 7230, pp. 706–710, 2009.

[34] S. Bhaviripudi, X. Jia, M. S. Dresselhaus, and J. Kong, “Role of kinetic factors in chemical vapor deposition synthesis of uniform large area graphene using copper catalyst,” *Nano Letters*, vol. 10, no. 10, pp. 4128–4133, 2010.

[35] E. Loginova, N. C. Bartelt, P. J. Feibelman, and K. F. McCarty, “Factors influencing graphene growth on metal surfaces,” *New Journal of Physics*, vol. 11, no. 6, p. 063046, 2009.

[36] I. Vlassiouk, M. Regmi, P. Fulvio, S. Dai, P. Datskos, G. Eres, and S. Smirnov, “Role of Hydrogen in Chemical Vapor Deposition Growth of Large Single-Crystal Graphene,” *ACS Nano*, vol. 5, no. 7, pp. 6069–6076, 2011.

[37] M. Batzill, “The surface science of graphene: Metal interfaces, CVD synthesis, nanoribbons, chemical modifications, and defects ,” *Surface Science Reports*, vol. 67, no. 3–4, pp. 83 – 115, 2012.

[38] L. Vicarelli, S. J. Heerema, C. Dekker, and H. W. Zandbergen, “Controlling Defects in Graphene for Optimizing the Electrical Properties of Graphene Nanodevices,” *ACS Nano*, vol. 9, no. 4, pp. 3428–3435, 2015.

[39] X. Li, C. W. Magnuson, A. Venugopal, J. An, J. W. Suk, B. Han, M. Borysiak, W. Cai, A. Velamakanni, Y. Zhu, L. Fu, E. M. Vogel, E. Voelkl, L. Colombo, and R. S. Ruoff, “Graphene films with large domain size by a two-step chemical vapor deposition process,” *Nano Letters*, vol. 10, no. 11, pp. 4328–4334, 2010.

[40] H. Kim, C. Mattevi, M. R. Calvo, J. C. Oberg, L. Artiglia, S. Agnoli, C. F. Hirjibehedin, M. Chhowalla, and E. Saiz, “Activation energy paths for graphene nucleation and growth on Cu,” *ACS Nano*, vol. 6, no. 4, pp. 3614–3623, 2012.

[41] G. López and E. J. Mittemeijer, “The solubility of C in solid Cu,” *Scripta Materialia*, vol. 51, no. 1, pp. 1–5, 2004.

[42] J. M. Wofford, S. Nie, K. F. McCarty, N. C. Bartelt, and O. D. Dubon, “Graphene islands on Cu foils: The interplay between shape, orientation, and defects,” *Nano Letters*, vol. 10, no. 12, pp. 4890–4896, 2010.

[43] X. Li, W. Cai, L. Colombo, and R. S. Ruoff, “Evolution of Graphene Growth on Ni and Cu by Carbon Isotope Labeling,” *Nano Letters*, vol. 12, no. 1, 2009.

[44] L. Fan, J. Zou, Z. Li, X. Li, K. Wang, J. Wei, M. Zhong, D. Wu, Z. Xu, and H. Zhu, “Topology evolution of graphene in chemical vapor deposition, a combined theoretical/experimental approach toward shape control of graphene domains,” *Nanotechnology*, vol. 23, no. 11, p. 115605, 2012.

[45] Y. N. Trehan, “The Reduction of Copper Oxides by Molecular Hydrogen,” *Zeitschrift für anorganische und allgemeine Chemie*, vol. 318, no. 1-2, pp. 107–112, 1962.

[46] K. L. Chavez and D. W. Hess, “A Novel Method of Etching Copper Oxide Using Acetic Acid,” *Journal of The Electrochemical Society*, vol. 148, no. 11, pp. G640–G643, 2001.

[47] J. Kang, D. Shin, S. Bae, and B. H. Hong, "Graphene transfer: key for applications," *Nanoscale*, vol. 4, pp. 5527–5537, 2012.

[48] J. Lee, C. Park, and G. Whitesides, "Solvent Compatibility of Poly(dimethylsiloxane)-Based Microfluidic Devices," *Analytical Chemistry*, vol. 75, no. 23, pp. 6544–6554, 2003.

[49] S. J. Kang, B. Kim, K. S. Kim, Y. Zhao, Z. Chen, G. H. Lee, J. Hone, P. Kim, and C. Nuckolls, "Inking Elastomeric Stamps with Micro-Patterned, Single Layer Graphene to Create High-Performance OFETs," *Advanced Materials*, vol. 23, no. 31, pp. 3531–3535, 2011.

[50] L. Jiao, B. Fan, X. Xian, Z. Wu, J. Zhang, and Z. Liu, "Creation of Nanostructures with Poly(methyl methacrylate)-Mediated Nanotransfer Printing," *Journal of the American Chemical Society*, vol. 130, no. 38, pp. 12612–12613, 2008.

[51] A. Reina, H. Son, L. Jiao, B. Fan, M. S. Dresselhaus, Z. Liu, and J. Kong, "Transferring and Identification of Single- and Few-Layer Graphene on Arbitrary Substrates," *The Journal of Physical Chemistry C*, vol. 112, no. 46, pp. 17741–17744, 2008.

[52] X. Li, W. Cai, J. An, S. Kim, J. Nah, D. Yang, R. Piner, A. Velamakanni, I. Jung, E. Tutuc, S. K. Banerjee, L. Colombo, and R. S. Ruoff, "Large-Area Synthesis of High-Quality and Uniform Graphene Films on Copper Foils," *Science*, vol. 324, no. 5932, pp. 1312–1314, 2009.

[53] X. Li, Y. Zhu, W. Cai, M. Borysiak, B. Han, D. Chen, R. D. Piner, L. Colombo, and R. S. Ruoff, "Transfer of Large-Area Graphene Films for High-Performance Transparent Conductive Electrodes," *Nano Letters*, vol. 9, no. 12, pp. 4359–4363, 2009.

[54] A. Pirkle, J. Chan, A. Venugopal, D. Hinojos, C. W. Magnuson, S. McDonnell, L. Colombo, E. M. Vogel, R. S. Ruoff, and R. M. Wallace, "The effect of chemical residues on the physical and electrical properties of chemical vapor deposited graphene transferred to SiO2," *Applied Physics Letters*, vol. 99, no. 12, 2011.

[55] J. Kedzierski, P.-L. Hsu, A. Reina, J. Kong, P. Healey, P. Wyatt, and C. Keast, "Graphene-on-Insulator Transistors Made Using C on Ni Chemical-Vapor Deposition," *Electron Device Letters, IEEE*, vol. 30, no. 7, pp. 745–747, 2009.

[56] K. T. He, J. D. Wood, G. P. Doidge, E. Pop, and J. W. Lyding, "Scanning Tunneling Microscopy Study and Nanomanipulation of Graphene-Coated Water on Mica," *Nano Letters*, vol. 12, no. 6, pp. 2665–2672, 2012.

[57] Y.-C. Lin, C. Jin, J.-C. Lee, S.-F. Jen, K. Suenaga, and P.-W. Chiu, "Clean Transfer of Graphene for Isolation and Suspension," *ACS Nano*, vol. 5, no. 3, pp. 2362–2368, 2011.

[58] J. Chan, A. Venugopal, A. Pirkle, S. McDonnell, D. Hinojos, C. W. Magnuson, R. S. Ruoff, L. Colombo, R. M. Wallace, and E. M. Vogel, "Reducing Extrinsic Performance-Limiting Factors in Graphene Grown by Chemical Vapor Deposition," *ACS Nano*, vol. 6, no. 4, pp. 3224–3229, 2012.

[59] Z. Cheng, Q. Zhou, C. Wang, Q. Li, C. Wang, and Y. Fang, "Toward Intrinsic Graphene Surfaces: A Systematic Study on Thermal Annealing and Wet-Chemical Treatment of SiO2-Supported Graphene Devices," *Nano Letters*, vol. 11, no. 2, pp. 767–771, 2011.

[60] J. D. Caldwell, T. J. Anderson, J. C. Culbertson, G. G. Jernigan, K. D. Hobart, F. J. Kub, M. J. Tadjer, J. L. Tedesco, J. K. Hite, M. A. Mastro, R. L. Myers-Ward, J. Charles R. Eddy, P. M. Campbell, and D. K. Gaskill, "Technique for the Dry Transfer of Epitaxial Graphene onto Arbitrary Substrates," *ACS Nano*, vol. 4, no. 2, pp. 1108–1114, 2010.

[61] S. H. Ahn and L. J. Guo, "High-Speed Roll-to-Roll Nanoimprint Lithography on Flexible Plastic Substrates," *Advanced Materials*, vol. 20, no. 11, pp. 2044–2049, 2008.

[62] R. Yerushalmi, Z. A. Jacobson, J. C. Ho, Z. Fan, and A. Javey, "Large scale, highly ordered assembly of nanowire parallel arrays by differential roll printing," *Applied Physics Letters*, vol. 91, no. 20, 2007.

[63] Y.-K. Chang and F. C.-N. Hong, "The fabrication of ZnO nanowire field-effect transistors by roll-transfer printing," *Nanotechnology*, vol. 20, no. 19, p. 195302, 2009.

[64] S. Bae, H. Kim, Y. Lee, X. Xu, J.-S. Park, Y. Zheng, J. Balakrishnan, T. Lei, H. Ri Kim, Y. I. Song, Y.-J. Kim, K. S. Kim, B. Ozyilmaz, J.-H. Ahn, B. H. Hong, and S. Iijima, "Roll-to-roll production of 30-inch graphene films for transparent electrodes," *Nature Nanotechnology*, vol. 5, no. 8, pp. 574–578, 2010.

[65] J. Kang, S. Hwang, J. H. Kim, M. H. Kim, J. Ryu, S. J. Seo, B. H. Hong, M. K. Kim, and J.-B. Choi, "Efficient Transfer of Large-Area Graphene Films onto Rigid Substrates by Hot Pressing," *ACS Nano*, vol. 6, no. 6, pp. 5360–5365, 2012.

[66] C.-Y. Su, A.-Y. Lu, C.-Y. Wu, Y.-T. Li, K.-K. Liu, W. Zhang, S.-Y. Lin, Z.-Y. Juang, Y.-L. Zhong, F.-R. Chen, and L.-J. Li, "Direct Formation of Wafer Scale Graphene Thin Layers on Insulating Substrates by Chemical Vapor Deposition," *Nano Letters*, vol. 11, no. 9, pp. 3612–3616, 2011.

[67] S.-J. Byun, H. Lim, G.-Y. Shin, T.-H. Han, S. H. Oh, J.-H. Ahn, H. C. Choi, and T.-W. Lee, "Graphenes Converted from Polymers," *The Journal of Physical Chemistry Letters*, vol. 2, no. 5, pp. 493–497, 2011.

[68] A. Ismach, C. Druzgalski, S. Penwell, A. Schwartzberg, M. Zheng, A. Javey, J. Bokor, and Y. Zhang, "Direct Chemical Vapor Deposition of Graphene on Dielectric Surfaces," *Nano Letters*, vol. 10, no. 5, pp. 1542–1548, 2010.

[69] W.-H. Lin, T.-H. Chen, J.-K. Chang, J.-I. Taur, Y.-Y. Lo, W.-L. Lee, C.-S. Chang, W.-B. Su, and C.-I. Wu, "A Direct and Polymer-Free Method for Transferring Graphene Grown by Chemical Vapor Deposition to Any Substrate," *ACS Nano*, vol. 8, no. 2, pp. 1784–1791, 2014.

[70] B. M. Trafas, Y.-N. Yang, R. L. Siefert, and J. H. Weaver, "Scanning tunneling microscopy of Ag growth on GaAs(110) at 300 K: From clusters to crystallites," *Phys. Rev. B*, vol. 43, pp. 14107–14114, 1991.

[71] G. Bennig, "Atomic force microscope and method for imaging surfaces with atomic resolution," Feb. 9 1988. US Patent 4,724,318.

[72] "Atomic Force Microscopy." Retrieved from http://education.mrsec.wisc.edu/nanoquest/afm/ on November 15th, 2015.

[73] G. Binnig, C. F. Quate, and C. Gerber, "Atomic Force Microscope," *Phys. Rev. Lett.*, vol. 56, pp. 930–933, 1986.

[74] Q. Zhong, D. Inniss, K. Kjoller, and V. Elings, "Fractured polymer/silica fiber surface studied by tapping mode atomic force microscopy," *Surface Science Letters*, vol. 290, no. 1, pp. L688 – L692, 1993.

[75] H. Hölscher, "AFM, Tapping Mode," in *Encyclopedia of Nanotechnology* (B. Bhushan, ed.), pp. 99–99, Springer Netherlands, 2012.

[76] N. A. Geisse, "AFM and combined optical techniques," *Materials Today*, vol. 12, no. 7–8, pp. 40 – 45, 2009.

[77] "NanoScope Analysis1.50," *Bruker*, 2015.

Appendix A

Particle and roughness analysis tables

A.1 Standard PMMA transfer

A.1.1 Particle analysis

						Average	*Standard Deviation*
Particle density (μm^2)	1,88	2,24	1,72	2,28	1,84	1,992	0,252

Table A.1: Particle density data retrieved from AFM images from CVD graphene transfered by the standard PMMA method.

A.1.2 Roughness analysis

Image roughness parameters

	Z Range	**Rq**	**Ra**
	57,500	1,940	1,130
	234,000	6,970	3,470
	30,300	0,812	0,762
Average	**107,267**	**3,241**	**1,787**
σ	90,299	2,677	1,199

Table A.2: Image roughness parametes retrieved from AFM images from CVD graphene transfered by the standard PMMA method.

Section roughness parameters

	Z range (nm)	Rq (nm)	Ra (nm)
	10,200	1,370	0,996
	19,200	1,190	0,751
	13,400	1,350	0,967
	8,250	0,813	0,627
	8,730	0,989	0,736
	22,500	2,800	2,210
	19,600	2,720	2,110
	20,100	2,810	2,120
	26,200	2,820	2,090
	28,300	2,850	2,090
	8,400	0,812	0,636
	10,700	0,910	0,676
	7,090	0,796	0,624
	7,670	0,849	0,654
	7,230	0,870	0,683
Average	**14,505**	**1,597**	**1,198**
σ	7,411	0,899	0,687

Table A.3: Section roughness parametes retrieved from AFM images from CVD graphene transfered by the standard PMMA method.

A.2 Transfer with extra HCl cleaning steps

A.2.1 Particle analysis

			Average	*Standard deviation*
Particle density (μm^2)	0,48	0,4	0,44	0,04

Table A.4: Particle density data retrieved from AFM images from CVD graphene transfered by the PMMA method, with a modified HCl cleaning.

A.2.2 Roughness analysis

Image roughness parameters

Z Range	Rq	Ra
58,800	1,450	0,843

Table A.5: Image roughness parameters data retrieved from AFM images from CVD graphene transfered by the PMMA method, with a modified HCl cleaning.

Section roughness parameters

	Z range	Rq	Ra
	8,670	0,974	0,787
	13,400	1,010	0,720
	6,620	0,771	0,614
	10,400	0,992	0,781
	6,800	0,769	0,613
Average	**9,178**	**0,9032**	**0,703**
σ	2,521	0,109	0,077

Table A.6: Section roughness parameters data retrieved from AFM images from CVD graphene transfered by the PMMA method, with a modified HCl cleaning.

A.3 Double layer transfer

A.3.1 Particle analysis

							Average	*Standard deviation*
Particle density (μm^2)	1,64	1,75	1,67	1,59	1,86	1,96	1,745	0,142

Table A.7: Particle density data retrieved from AFM images from CVD graphene transfered by the PMMA method, with a polymer double layer.

A.3.2 Roughness analysis

Image roughness parameters

	Z Range	Rq	Ra
	50,200	1,760	1,060
	39,600	1,260	0,837
	69,100	1,980	1,180
	52,700	1,600	0,920
	81,800	1,630	0,832
Average	**80,900**	**2,590**	**1,197**
σ	56,439	2,324	0,581

Table A.8: Image roughness parameters data retrieved from AFM images from CVD graphene transfered with an additional PMMA layer.

Section roughness parameters

	Z range	Rq	Ra
	10,800	1,130	0,879
	15,000	1,130	0,851
	20,600	1,350	0,871
	8,760	1,040	0,829
	11,400	1,120	0,820
	11,600	1,010	0,788
	10,600	0,979	0,775
	8,750	0,960	0,766
	12,500	1,150	0,838
	16,400	1,180	0,859
	13,400	1,190	0,871
	34,300	2,020	1,060
	12,500	1,020	0,801
	12,500	1,050	0,819
	10,100	0,973	0,750
	9,900	0,990	0,779
	9,450	0,772	0,595
	7,560	0,787	0,595
	12,700	0,920	0,665
	13,100	1,030	0,784
	12,700	0,920	0,662
	6,850	0,809	0,626
	11,500	0,838	0,606
	8,310	0,751	0,568
	7,990	0,764	0,584
	11,600	0,846	0,636
Average	**12,341**	**1,028**	**0,757**
σ	5,357	0,253	0,121

Table A.9: Section roughness parameters data retrieved from AFM images from CVD graphene transfered with an additional PMMA layer.

A.4 Transfer with baking after spin coating

A.4.1 Particle analysis

							Average	*Standard deviation*
Particle density (μm^2)	0,72	1,34	0,96	1,15	1,27	0,96	1,067	0,231

Table A.10: Particle density data obtained from AFM images of CVD graphene transfered by the PMMA method, with a baking step after spin coating.

A.4.2 Roughness analysis

Image roughness parameters

	Z Range	Rq	Ra
	24,800	0,655	0,376
	31,900	1,250	0,623
	21,900	0,742	0,426
	24,000	0,814	0,437
	21,400	0,763	0,493
	31,800	1,210	0,663
Average	**25,967**	**0,906**	**0,503**
σ	4,730	0,257	0,115

Table A.11: Image roughness parameters data retrieved from AFM images from CVD graphene transfered with a baking after spin coating.

Section roughness parameters

	Z range	Rq	Ra
	4,950	0,358	0,253
	4,500	0,315	0,236
	4,900	0,359	0,252
	5,340	0,476	0,312
	11,100	0,676	0,386
	4,800	0,376	0,271
	5,800	0,394	0,270
	5,660	0,416	0,283
	6,790	0,501	0,311
	8,160	0,497	0,278
	6,540	0,399	0,254
	5,410	0,407	0,289
	5,050	0,412	0,313
	4,230	0,391	0,301
	3,930	0,374	0,293
	6,180	0,432	0,308
	5,420	0,592	0,442
	4,670	0,396	0,303
	11,300	0,654	0,514
	5,070	0,393	0,303
	5,500	0,392	0,289
	5,350	0,422	0,308
	4,220	0,425	0,322
	5,770	0,454	0,317
Average	**5,860**	**0,438**	**0,309**
σ	1,881	0,090	0,061

Table A.12: Section roughness parameters data retrieved from AFM images from CVD graphene transfered with a baking after spin coating.

A.5 Baking after transfer to substrate

A.5.1 Particle analysis

						Average	*Standard deviation*
Particle density (μm^2)	1,02	0,72	0,72	0,81	0,29	0,712	0,238

Table A.13: Particle density data obtained from AFM images of CVD graphene transfered by the PMMA method, with baking step after films' transfer to the final substrate.

A.5.2 Roughness analysis

Image roughness parameters

	Z Range	**Rq**	**Ra**
	50,000	1,360	0,636
	50,200	1,640	0,889
	61,900	1,570	0,789
	186,000	4,120	0,983
	194,000	3,590	0,910
Average	**108,420**	**2,456**	**0,841**
σ	74,681	1,295	0,134

Table A.14: Image roughness parameters data retrieved from AFM images from CVD graphene PMMA method, with baking step after films' transfer to the final substrate.

Section roughness parameters

	Z range	Rq	Ra
	6,540	0,537	0,406
	6,400	0,527	0,402
	6,440	0,696	0,553
	7,430	0,648	0,502
	13,400	0,806	0,559
	16,800	0,923	0,622
	10,500	0,882	0,635
	13,600	1,050	0,705
	9,390	0,797	0,597
	11,500	0,790	0,592
	10,300	0,834	0,609
	13,600	0,951	0,685
	6,800	0,702	0,545
	6,020	0,705	0,549
	8,280	0,632	0,494
	5,780	0,674	0,527
	7,110	0,811	0,607
	8,530	3,590	0,910
	5,970	0,808	0,638
	8,670	0,824	0,620
Average	**9,153**	**1,508**	**0,694**
σ	3,178	1,388	0,145

Table A.15: Section roughness parameters data retrieved from AFM images from CVD graphene PMMA method, with baking step after films' transfer to the final substrate.

A.6 Baking after transfer to substrate and annealing

A.6.1 Particle analysis

						Average	*Standard deviation*
Particle density (μm^2)	0,19	0,21	0,26	0,37	0,11	0,228	0,096

Table A.16: Particle density data obtained from AFM images of CVD graphene transfered by the PMMA method, with a baking step after films' transfer to the final substrate and annealing after acetone bath.

A.6.2 Roughness analysis

Image roughness parameters

	Z range	Rq	Ra
	31,600	1,040	0,560
	42,400	0,772	0,453
	20,000	0,529	0,336
	21,900	0,731	0,435
	30,500	0,806	0,506
	30,600	0,786	0,500
Average	**29,500**	**0,777**	**0,465**
σ	8,013	0,164	0,077

Table A.17: Section roughness parameters data retrieved from AFM images from CVD graphene PMMA method, with baking step after films' transfer to the final substrate and annealing.

Section roughness parameters

	Z range	Rq	Ra
	10,200	0,455	0,328
	8,170	0,508	0,334
	6,140	0,491	0,337
	14,800	0,615	0,329
	5,670	0,421	0,317
	6,210	0,519	0,380
	6,460	0,552	0,402
	6,990	0,461	0,310
	8,090	0,528	0,356
	8,620	0,441	0,284
	9,870	0,396	0,263
	4,320	0,338	0,250
	14,300	0,553	0,310
	7,560	0,434	0,288
	10,700	0,449	0,290
	5,610	0,446	0,321
	9,250	0,517	0,360
	7,810	0,379	0,263
	13,400	0,560	0,350
	7,140	0,444	0,298
	7,630	0,534	0,373
	8,090	0,579	0,386
	7,240	0,584	0,391
	7,930	0,632	0,444
	8,140	0,652	0,442
	9,770	0,584	0,390
Average	**4,484**	**0,421**	**0,338**
σ	2,645	0,081	0,051

Table A.18: Image roughness parameters data retrieved from AFM images from CVD graphene PMMA method, with baking step after films' transfer to the final substrate and annealing.

A.7 Double layer transfer and annealing

A.7.1 Particle analysis

						Average	*Standard deviation*
Particle density (μm^2)	0,32	1,02	0,86	0,27	0,15	0,575	0,389

Table A.19: Particle density data obtained from AFM images of CVD graphene transfered by the PMMA method, with a polymer double layer and annealing after acetone bath.

A.7.2 Roughness analysis

Image roughness parameters

	Z range	Rq	Ra
	66,600	2,090	1,110
	96,000	2,060	1,100
	31,100	0,932	0,500
	73,500	1,470	0,827
	25,000	0,734	0,800
Average	**58,440**	**1,457**	**0,867**
σ	26,720	0,559	0,225

Table A.20: Image roughness parameters data retrieved from AFM images from CVD graphene transfered with an additional PMMA layer and an annealing step after the acetone bath.

Section roughness parameters

	Z range	Rq	Ra
	11,500	1,240	0,960
	7,950	1,240	1,010
	7,480	1,130	0,918
	6,790	1,120	0,908
	8,890	1,200	0,957
	9,840	1,100	0,827
	6,350	0,910	0,714
	9,070	0,835	0,566
	6,210	0,879	0,662
	6,610	0,973	0,774
	6,510	0,546	0,390
	6,500	0,533	0,389
	8,230	0,612	0,431
	14,300	0,770	0,462
	13,300	0,619	0,413
	10,200	0,962	0,683
	9,380	0,972	0,673
	8,230	1,010	0,682
	11,800	0,875	0,596
	8,810	0,734	0,506
	8,830	0,942	0,631
	9,130	1,040	0,701
	8,130	0,904	0,560
	9,450	0,958	0,640
Average	**8,895**	**0,921**	**0,669**
Std Deviation	2,149	0,206	0,189

Table A.21: Section roughness parameters data retrieved from AFM images from CVD graphene transfered with an additional PMMA layer and an annealing step after the acetone bath.